Sniffing can be initiated by dopamine's actions on ventral striatum neurons

Natalie L. Johnson[1], Anamaria Cotelo-Larrea[1], Lucas A. Stetzik[1], Umit M. Akkaya[2], Zihao Zhang[1], Marie A. Gadziola[3], Adrienn G. Varga[4], Minghong Ma[5], and Daniel W. Wesson[1,*]

[1]Department of Pharmacology and Therapeutics, Center for Smell and Taste, Center for Addiction Research and Education; University of Florida College of Medicine, Gainesville, FL 32610, USA

[2]Department of Computer Engineering, Gebze Technical University, 41400 Kocaeli, Turkey

[3]Department of Psychology, University of Toronto Scarborough, Toronto, ON, Canada

[4]Department of Neuroscience, Breathing Research and Therapeutics Center; University of Florida College of Medicine, Gainesville, FL 32610, USA

[5]Department of Neuroscience, Perelman School of Medicine, University of Pennsylvania, Philadelphia, PA 19104, USA

[*]Corresponding author: Email: danielwesson@ufl.edu

Abstract

Sniffing is a motivated behavior displayed by nearly all terrestrial vertebrates. While sniffing is associated with acquiring and processing odors, sniffing is also intertwined with affective and motivated states. The neuromodulatory systems which influence the display of sniffing are unclear. Here, we report that dopamine release into the ventral striatum is coupled with bouts of sniffing and that stimulation of dopaminergic terminals in these regions drives increases in respiratory rate to initiate sniffing whereas inhibition of these terminals reduces respiratory rate. Both the firing of individual neurons and the activity of post-synaptic D1 and D2 receptor-expressing neurons in the ventral striatum are also coupled with sniffing and local antagonism of D1 and D2 receptors squelches sniffing. Together, these results support a model whereby sniffing can be initiated by dopamine's actions upon ventral striatum neurons. The nature of sniffing being integral to both olfaction and motivated behaviors implicates this circuit in a wide array of functions.

Introduction

Sniffing is a volitional behavior displayed by nearly all terrestrial vertebrates and is defined by the rapid inhalation and exhalation of air through the nose. The commonplace function ascribed to sniffing is that it aids in perceiving odors[1,2]. This is supported by studies reporting that rodents increase their respiratory frequency from ~2-4Hz at rest, up into an around 6-12Hz range when sampling an odor[3–6]. In addition to supporting olfaction, sniffing is also intertwined with affective and motivated states wherein sniffing is considered an appetitive behavior[7–9]. For instance, rodents, dogs, and even semi-aquatic vertebrates increase their sniffing frequency while foraging for food and in anticipation of reinforcers in instrumental tasks[5,6,9,10]. The frequency of sniffing also appears to influence emotional states[11,12]. Furthermore, sniffing serves as a "master clock" for essential physiological rhythms including whisking, wherein the rhythm of sniffing is coupled with whisking and also other head movements[13,14]. Therefore, it is clear that sniffing holds a ubiquitous position in nature.

The automatic coordination of respiration, and the tight control of the inspiratory / post-inspiratory / expiratory rhythm, are afforded by brainstem structures which elegantly time breaths, control their depth, and send these instructive signals toward the breathing plant by means of the spinal and cranial nerves[15,16]. While likely many of the respiratory brainstem structures that participate in the control of basal breathing are integral for the orchestration of sniffing, the exact mechanisms and neural basis for sniffing still remain unknown. Although sniffing is associated with increased bursting in the inspiratory rhythm generator, the pre-Bötzinger complex[17], optogenetic stimulation of this region has yet to reproduce the rapid breathing rates that characterize sniffing[18–20], unlike a

63 subset of neurons in the pontine respiratory modulator, parabrachial nucleus[21]. Additionally,
64 subsets of neurons in the expiratory control center, the retrotrapezoid nucleus, increase their
65 activity shortly before the onset of sniffing[22]. These neurons provide input to the pre-Bötzinger
66 complex[23], as well as the facial motor nucleus, another region recognized to play a direct role in
67 controlling sniffing[24]. While these findings together begin to uncover the circuitry for sniffing,
68 more work needs to be done to pinpoint all the components, and specifically the neuromodulatory
69 circuitry, which invigorates an animal to go from basal breathing which serves the purpose of gas
70 exchange, to engage in the voluntary act of sniffing.
71
72 We reasoned the mesolimbic dopamine (DA) system as a prime candidate for the invigoration of
73 sniffing. Electrical stimulation of the ventral tegmental area (VTA) elicits vigorous sniffing[25].
74 Neurons synthesizing DA in the VTA project into the basal forebrain, including into the ventral
75 striatum. The ventral striatum, considered a limbic-motor interface[26], is well-known to integrate
76 cortical and limbic circuitry to adaptively guide behavior[27,28]. The major subcomponents of the
77 ventral striatum, including the nucleus accumbens (NAc) and the tubular striatum (TuS; also
78 known as the olfactory tubercle) are recipient of dense DAergic inputs from the VTA. Neurons in
79 both the NAc and TuS are largely spiny projection neurons expressing D1- or D2-like receptors
80 which mediate actions of DA[29–31].
81
82 Through studies of DA's role in the ventral striatum, we have come to learn that DA's actions in
83 the ventral striatum influence a wide-range of behaviors and states, such as aversion behaviors,
84 and also cellular plasticity needed for learning[32–37]. DA in the ventral striatum is also a major
85 mediator of motivated states and reinforcement with manipulation of DA, and D1 and D2 neural

activity in the ventral striatum guiding those functions[36,38–40]. Since sniffing is a motivated behavior, it is reasonable to believe the ventral striatum's role in motivational control is in-part a regulatory system which influences the occurrence of sniffing. Indeed, DAergic manipulations in the ventral striatum also influence exploratory behaviors in open-field and other gross motor behavior assays and recently it was reported that DAergic inputs regulate whisking[41]. Mesolimbic DA thus seems a quintessential neural system for supporting sniffing. Here, we investigated the role of mesolimbic DA in the display of sniffing behavior to find that sniffing can be initiated by DA's actions upon ventral striatum neurons.

Results

Sniffing frequency is associated with mesolimbic DA release

We initially sought to understand the relationship between sniffing and DA release in the ventral striatum. To address this, we first performed a tracing study to identify ventral striatum subregions wherein DA inputs terminate for subsequent monitoring of DA during behavior. It is well known in both mice and rats that the ventral striatum receives dense input from mesolimbic DAergic neurons[28,42,43] and that DA dynamics may differ between ventral striatum subregions[44,45]. In contrast to the innervation of the dorsal striatum and NAc, quantitative analyses of DA input to the TuS in mice is especially lacking. To address this, we injected AAV1-hSyn-FLEX-mGFP-2A-Synaptophysin-mRuby into the VTA of *DAT^{IRES}-Cre* mice (**Fig 1A & Supplementary Fig 1**). This approach allowed for visualization of fluorescent puncta, which indicate DAergic presynaptic terminals, throughout the TuS and NAc (**Fig 1B**). The injections resulted in GFP expression throughout the VTA (**Supplementary Fig 1**). We quantified fluorescent puncta in the NAc Core (NAcC), NAc Shell (NAcSh), medial TuS (mTuS), and lateral TuS given different roles for these

109 subregions in the regulation of motivated behaviors (**Fig 1C**)[46–49]. As expected, we observed robust
110 fluorescence, indicating synaptophysin+ DAT VTA terminals, in the TuS and NAc, most notably
111 in the anterior aspect of the mTuS and NAc (**Fig 1C**) with 113% and 78% more innervation in the
112 anterior versus posterior halves of the mTuS and NAcSh, respectively (the anterior or posterior-
113 most 200µm were used for quantification of these regions). Following this we focused analyses on
114 the anterior aspect of both structures. While the mTuS was rich with synaptophysin+ DAT VTA
115 terminals, this contrasted to the lateral TuS which was largely void of innervation (**Fig 1C & 1D**,
116 rmANOVA $F(1.52, 7.6)=31.74$ $p=0.0003$, Tukey's multiple comparisons ant mTuS vs. ant LatTuS
117 $p=0.014$). Comparable amounts of synaptophysin+ DAT VTA terminals were found in the anterior
118 NAcSh and anterior NAcC (**Fig 1C & 1D**, Tukey's multiple comparisons antNAcSh vs. antNAcC,
119 $p=0.073$). The density of input across the anteromedial aspects of the TuS, NAcSh, and NAcC
120 were all similar (**Fig 1C & 1D;** Tukey's multiple comparisons anterior mTuS vs. anterior NAcSh
121 $p=0.217$; anterior mTuS vs. anterior NAcC $p=0.878$). Together this work adds to literature
122 indicating that the anterior NAcSh, NAcC, and mTuS are the major recipients of VTA DAergic
123 input in the ventral striatum and provide quantitative support for focusing on the medial aspects of
124 these regions in mice.
125
126 Having established this, we next sought to investigate the temporal relationship between
127 mesolimbic DA release and sniffing behavior. We took advantage of whole-body
128 plethysmography to assess respiratory cycles in awake mice and identify bouts of sniffing. In this
129 method, breaths are detected by a pressure transducer which accesses the inside of the chamber
130 (**Fig 2A**). The technical needs of our experiments require a patch cable attached to the mouse in
131 the chamber (*e.g.,* **Fig 2C**) which may impair fidelity of the respiratory signal since the cable

132 would need to exit the plethysmography chamber which is normally air-tight. Further, we wished
133 to identify temporal relationships between sniffing and other signals (DA, photostimulation, *etc*)
134 and this mandates that first we establish a temporal relationship between breaths detected with
135 whole-body plethysmography and breathing of mice which occurs only through their noses since
136 they are obligate nasal air breathers. Therefore, we simultaneously monitored respiration via the
137 plethysmograph as well as by means of a chronically-implanted cannula into the dorsal nasal recess
138 of awake mice (**Fig 2A**)[6]. For the intranasal measures, a flexible tube was connected to the nasal
139 cannula which passed through the top of the plethysmograph via a snug 3D-printed fitting which
140 allowed for mice to explore and freely-rotate within the plethysmograph. The end of this tube
141 terminated into a pressure transducer for amplification of intranasal pressure changes. Using this
142 simultaneous approach, we confirmed in three mice that whole-body plethysmography, even with
143 the patch cable freely passing through the chamber, reliably detected intranasal respiratory cycles,
144 and faithfully followed during high frequency sniffing bouts (**Fig 2Bi & 2Biii**). The only notable
145 difference we observed for the purpose of this study was a slight temporal lag with the peaks of
146 the whole-body plethysmograph signal trailing those of the intranasal signal (**Fig 2Bii**). This lag
147 is anticipated since the origin of the signal is from within the mouse (intranasal) versus from within
148 a chamber (plethysmograph). Across the three mice as they spontaneously transition in and out of
149 sniffing bouts, the mean lag ranged from 0.028 ± 0.007s to .036 ± 0.0004s (using data with
150 respiratory rates ranging from ~2-12Hz, as in **Fig 3Biii**). While solely at resting respiration (2-
151 4Hz), the lag between the two signals increased and ranged from 0.053 ± 0.001s to 0.10 ± 0.001s
152 (across-animal range). Nevertheless, in events wherein respiratory cycles were detected in the
153 nose, in >99% of the cases, they were also detected by the plethysmograph (3,239 breaths across
154 three mice, a restricted range of data from one mouse shown in **Fig 2Bii**).

155

156 Having confirmed the ability to accurately detect both individual respiratory cycles and sniffing
157 bouts alike, we next monitored the relationship between DA levels in the ventral striatum as they
158 relate to sniffing. We injected mice into either the medial TuS, the NAcSh, or NAcC with an AAV
159 encoding $GRAB_{DA}$ (pAAV.hSyn-GRAB_DA1h)[50] and in the same surgery implanted into the
160 structure receiving the AAV, a 400µm optical fiber for later fiber photometry. Other than for the
161 purpose of showing example traces, for other analyses we subtracted the isosbestic 405nm signal
162 from the $GRAB_{DA}$ signal. Following several weeks for surgical recovery and viral expression, we
163 placed the mice in a plethysmograph for simultaneous monitoring of respiration and DA levels
164 (**Fig 2C**). Since mice rapidly transition in and out of sniffing bouts[6], we restricted our analyses to
165 more stable/pronounced bouts versus short bouts by only defining a sniff bout as the occurrence
166 of sniffing ≥6Hz for ≥1s in duration. Further, in some instances, mice continuously sniff for
167 numerous seconds and then reengage in another bout shortly thereafter. Since these may reflect
168 periods of more generalized arousal versus spontaneous exploratory behavior, we excluded sniff
169 bouts occurring in proximity to these long (>10s) sniffing bouts. We analyzed the relationship
170 between DA levels and sniffing in several manners, and in all analyses, we accounted for the lag
171 between when a nasal inhalation occurs and when the plethysmograph detects the inhalation by
172 subtracting the conservative 28ms lag (see **Fig 2Bii**) from the onset event of every peak-detected
173 respiratory cycle.

174

175 We analyzed DA levels across trials wherein mice in the plethysmograph spontaneously sniffed,
176 were delivered odors to evoke sniffing, or were delivered an auditory/somatosensory stimulus by
177 connecting a vibration motor to the plethysmograph which modestly resonated the chamber while

178 simultaneously providing a small auditory 'buzz' cue due to its motor (**Supplementary Fig 2**). All
179 mice were confirmed to have implants extending into the mTuS, NAcC, or the NAcSh (**Fig 2D**).
180
181 First, we looked at the relationship between spontaneous sniffing like that displayed by mice
182 during self-motivated states of exploration. As shown in the example traces from a mouse
183 implanted into the TuS (**Fig 2E**), whereas no detectable changes in DA levels were observed when
184 mice were simply breathing at baseline frequencies ('respiration at rest'; **Fig 2Ei &**
185 **Supplementary Fig 3A**), spontaneous sniffing was associated with elevations in the $GRAB_{DA}$
186 signal (**Fig 2Eii**). Across mice, $GRAB_{DA}$ levels during spontaneous sniffing were elevated in both
187 the TuS and the NAcSh, but in contrast were decreased in the NAcC (**Fig 2Fi, 2Gi, 2Hi**; TuS
188 paired $t(6)=11.85$ $p<0.0001$; NAcSh paired $t(6)=6.56$, $p=0.0006$; NAcC paired $t(6)=12.15$,
189 $p<0.0001$). Only in the TuS, was the average frequency of the spontaneous sniffing bout correlated
190 with the amplitude of the $GRAB_{DA}$ signal (**Fig 2Fii, 2Gii, & 2Hii;** TuS Pearson's $r(83)=0.29$,
191 $p=0.008$), but not in the NAcSh or NAcC (NAcSh Pearson's $r(101)=0.12$, $p=0.2493$; NAcC
192 Pearson's $r(102)=0.038$, $p=0.703$). Notably, neither the isosbestic 405nm signal acquired from
193 these same animals, nor the DA-insensitive control virus, $GRAB_{DA}$-mut, acquired in a separate
194 cohort of 9 mice, showed comparable changes during spontaneous sniffing (**Supplementary Fig**
195 **4**).
196
197 Next, we investigated the relationship between odor-evoked sniffing and DA levels (**Fig 3A**). Each
198 mouse was presented with pseudorandom trials of odors, including R(+)-limonene, thioglycolic
199 acid, and peanut oil, each five times across a behavior session. These odors were selected based
200 upon their known positive hedonic qualities perceived by mice, in order to elicit vigorous sniffing

201 [51–53]. As shown in the example in **Figure 3B** from a mouse implanted in the TuS, the first
202 presentation of thioglycolic acid was associated with robust increases in sniffing, which was
203 accompanied by an increase in the $GRAB_{DA}$ signal. Across all groups (TuS, NAcSh, NAcC),
204 sniffing frequency was elevated compared to baseline for the first presentation of odors (TuS
205 paired $t(6)=19.23$, $p<0.0001$; NAcSh paired $t(6)=13.27$, $p<0.0001$; NAcC paired $t(6)=14.35$,
206 $p<0.0001$), which habituated across subsequent presentations (TuS rmANOVA
207 $F(2.26,13.55)=14.64$, $p=0.0003$; NAcSh rmANOVA $F(2.44, 14.65)=32.65$, $p<0.0001$; NAcC
208 rmANOVA $F(1.59, 9.55)=23.5$, $p=0.0003$) (**Figs 3Ci, 3Di, & 3Ei**). Simultaneously during novel
209 odor-evoked sniffing bouts (trial #1 of odor), we observed elevations in the $GRAB_{DA}$ signal in
210 both the TuS and NAcSh (**Fig 3Cii & 3Dii**; TuS paired $t(6)=6.54$, $p=0.0006$; NAcSh paired
211 $t(6)=4.38$, $p=0.005$). The increases rose soon around sniff bout onset and decayed within a few
212 seconds. In contrast, the NAcC displayed reduction in the $GRAB_{DA}$ signal upon sniffing (**Fig 3Eii**;
213 paired $t(6)=8.35$, $p=0.0002$).
214
215 The elevation in the $GRAB_{DA}$ signal was not solely due to odor input since the signal became
216 attenuated across repeated odor deliveries in the TuS and NAcSh **(Fig 3Ciii & 3Diii**; trials #1-5;
217 TuS rmANOVA $F(2.08, 12.48)=7.942$, $p=0.006$; NAcSh rmANOVA: $F(1.90,11.39)=5.563$,
218 $p=0.022$), whereupon trial 5, the $GRAB_{DA}$ signal was observed near baseline levels. In the NAcC,
219 reductions in the $GRAB_{DA}$ signal was not relieved with repeated odor presentations (**Fig 3Eiii**;
220 rmANOVA $F(1.98, 11.90)=0.5760$, $p=0.58$). Also supporting that the change in amplitude of the
221 $GRAB_{DA}$ signal is related to sniffing, we found that the frequency of odor-evoked sniffing
222 correlated with the peak of the $GRAB_{DA}$ signal in both the TuS and NAcSh (TuS Pearson's
223 $r(34)=0.65$, $p<0.0001$; NAcSh Pearson's $r(34)=0.51$, $p=0.002$), but not in the NAcC (Pearson's

224 $r(34)=-0.14$, $p=0.414$) (**Figs 3Civ, 3Div, & 3Eiv**). Interestingly here, the odor-evoked sniffing in
225 the NAcSh was correlated with $GRAB_{DA}$ levels which was not the case with spontaneous sniffing
226 (**Fig 2G**), suggesting in the NAcSh the relationship may be dependent upon odor.
227
228 Finally, we assessed the impact of the multimodal buzz stimulus on $GRAB_{DA}$ levels. While not as
229 dramatic nor reliable as an odor (as in **Fig 3Ci, 3Di, & 3Ei**), the buzz stimulus evoked sniffing
230 greater than baseline in the majority of mice (**Fig 3Fi, 3Gi, & 3Hi**). Correspondingly, DA was
231 elevated upon initial buzz-evoked sniffing in the TuS and the NAcSh (**Figs 3Fii & Gii**; TuS paired
232 $t(6)=6.77$, $p=0.0005$; NAcSh paired $t(6)=3.17$, $p=0.019$). The buzz-evoked sniffing did not
233 strongly habituate across repeated trials, and likewise, $GRAB_{DA}$ levels also remained consistent
234 across trials (**Fig 3Fi & 3Fiii**, **Fig 3Gi & 3Giii**; TuS sniffing rmANOVA $F(2.57, 15.4)=1.351$,
235 $p=0.293$; TuS $GRAB_{DA}$ rmANOVA $F(1.90, 11.38)=0.49$, $p=0.616$; NAcSh sniffing rmANOVA
236 $F(2.43, 14.58)=2.97$, $p=0.0752$; NAcSh $GRAB_{DA}$ rmANOVA $F(1.32, 7.94)=0.27$, $p=0.6786$).
237 Interestingly, in the NAcSh, there was a biphasic increase in $GRAB_{DA}$ with the first phase
238 occurring upon buzz onset, and the second upon buzz offset (**Fig 3Gii**). Whereas in the NAcSh,
239 $GRAB_{DA}$ levels measured upon either phase were not correlated with the frequency of sniffing
240 (**Fig 3Giv**; during buzz Pearson's $r(34)=-0.17$, $p=0.316$; upon buzz offset Pearson's $r(34)=-0.074$,
241 $p=0.673$), the $GRAB_{DA}$ levels upon buzz strongly correlated with frequency of sniffing in the TuS
242 (**Fig 3Eiv**; Pearson's $r(34)=0.43$, $p=0.011$). Similar to that seen for both spontaneous sniffing and
243 odor-evoked sniffing, $GRAB_{DA}$ levels in the NAcC were reduced upon buzz-evoked sniffing (**Fig**
244 **3Hii**; paired $t(6)=3.23$, $p=0.018$) which similarly did not habituate across trials (**Fig 3Hii & 3Hiii**;
245 rmANOVA $F(2.19, 13.14)=0.44$, $p=0.668$). There was no correlation between buzz-evoked
246 sniffing frequency and $GRAB_{DA}$ levels in the NAcC (**Fig 3Hiv**; Pearson's $r(34)=-0.22$, $p=0.194$).

247 When comparing the peak $GRAB_{DA}$ responses across all regions and all conditions, we found
248 similar evoked responses in the TuS and NAcSh to novel odor (trial #1 of odor) presentations and
249 during spontaneous sniffing **(Fig 3I**; two-way rmANOVA, main effect of region $F(2,18)=58.45$,
250 $p<0.0001$; Tukey's multiple comparisons TuS vs. NAcSh odor $p=0.99$; TuS vs. NAcSh spont
251 $p=0.219$). As with spontaneous sniffing, neither odor- nor buzz-evoked sniffing resulted in
252 comparable changes in the separate cohort of 9 mice wherein we recorded $GRAB_{DA}$-mut signal
253 (**Supplementary Fig 4**). Taken together, these results indicate that sniffing often corresponds with
254 increases in DA release in two specific sub-regions of the ventral striatum, and that the level of
255 DA correlates to the frequency of sniffing.
256
257 ***DA release into the ventral striatum elicits sniffing***
258 Given the relationship between DA release in the ventral striatum and the occurrence and
259 frequency of sniffing, we next sought to determine whether this release of DA is sufficient to elicit
260 sniffing. To assess this, we injected a Cre-dependent Channelrhodopsin2 (AAV5-EF1α-DIO-
261 hChR2(E123T/T159C)-EYFP) unilaterally into the VTA of DAT^{IRES}-*Cre* mice (**Supplementary**
262 **Fig 5**) and implanted a 300µm optical fiber terminating over the TuS, NAcSh, or NAcC to drive
263 terminal release of DA upon light stimulation (**Fig 4A & 4B**). Control mice were injected with
264 AAV solely expressing EYFP in the VTA (AAV5-EF1α-DIO-eYFP) and also received an optical
265 fiber terminating over the TuS, NAcSh, or NAcC. One second long, 25Hz 473nm light stimulation
266 was delivered through the optical fiber while mice were in the plethysmograph. This 25Hz stimulus
267 was selected based upon prior work using a similar stimulus paradigm to elicit VTA DA release
268 into the ventral striatum[39,40,54]. As shown in **Figure 4C**, in an example mouse, photostimulation of
269 DAergic terminals in the TuS evoked a brief bout of sniffing. In this example mouse, the average

latency to onset of a sniff bout was 240 ± 22.5ms (across trial range: 130-330ms; bout onset defined as the moment of achieving ≥6Hz respiration). Further, the average amount of time spent sniffing (time ≥6Hz) during photostimulation was 672 ± 59.6ms (across trial range: 310-1000ms). The light evoked sniffing in this example mouse was also reliable across repeated trials (**Fig 4C**).

In all three ChR2-injected groups of mice, we observed a rapid increase in respiratory frequency upon photostimulation (**Fig 4D**). This photostimulation-evoked display of sniffing was largely maintained across repeated trials (**Fig 4D & 4E;** testing for stability in Hz across trials: mixed-effects analysis $F(4.09, 85.87)=2.34$, $p=0.058$). While anticipated, EYFP control mice displayed a slight increase in respiratory frequency during photostimulation, likely due to the arousing nature of the visual stimulus leaking from the fiber implant. Alternatively, given that light stimuli can evoke DA release in the ventral striatum[55] it is also possible that light-triggered DA release could have contributed to the increase in respiratory frequency seen in EYFP controls. Nonetheless, the frequency of the sniffing bout was lower in EYFP mice than in all ChR2-treated groups (**Fig 4D, right, Fig 4E & F**). As shown in **Figure 4F**, the temporal dynamics of photostimulation-evoked sniffing in ChR2-injected mice was remarkedly similar. The average latency to onset of a sniff bout was 279.4 ± 13.3ms SEM (inter-mouse range: 225-362.5ms) for TuS, 264.7 ± 14.83ms SEM (inter-mouse range: 202.5-299ms) for NAcSh, and 263.3 ± 7.52ms SEM (inter-mouse range: 242.2-290ms) for NAcC (**Fig 4Gi**). The average latency to the onset of a sniff bout in EYFP controls (339.4 ± 18.72ms SEM, inter-mouse range: 274.2-405ms) was significantly greater than in the ChR2-treated groups (all groups with means <290ms as in **Fig 4Gi;** one-way ANOVA $F(3, 25)=5.11$, $p=0.007$, Tukey's multiple comparisons test TuS vs. EYFP $p=0.0273$, NAcSh vs. EYFP $p=0.0141$, NAcC vs. EYFP $p=0.122$). Further, the average amount of time spent sniffing during

293 photostimulation was 534.1 ± 37.8ms (inter-mouse range 314.3-743ms) for TuS, 647.7 ± 53.7ms
294 (inter-mouse range 479-834ms) for NAcSh, and 520.1 ± 85.7ms (inter-mouse range 254.4-755ms)
295 for NAcC. All ChR2-treated mice spent more time sniffing than EYFP controls, and there were no
296 significant differences between ChR2-treated groups (**Fig 4Gii**) (one-way ANOVA
297 $F(3,28)=14.02$, $p<0.0001$; Tukey's multiple comparisons test TuS vs. EYFP $p=0.0001$, NAcSh vs.
298 EYFP $p<0.0001$, NAcC vs. EYFP $p=0.0017$). Further, the frequency of photostimulation-evoked
299 sniffing (measured as the peak Hz during photostimulation) did not differ between ChR2-treated
300 groups and was significantly greater than EYFP controls (**Fig 4Giii**; one-way ANOVA $F(3,$
301 $28)=14.17$, $p<0.0001$; Tukey's multiple comparisons test TuS vs. EYFP $p<0.0001$, NAcSh vs.
302 EYFP $p<0.0001$; NAcC vs. EYFP $p=0.0010$). Finally, we explored the reliability whereby a
303 DAergic terminal photostimulation would elicit a sniffing bout. The probability that
304 photostimulation elicited sniffing was robust, and significantly greater than in EYFP controls –
305 indeed with many animals in each ChR2-treatment group displaying a sniff bout to *every*
306 photostimulation trial and the vast majority to >80% of trials (**Fig 4Giv**; one-way ANOVA $F(3,$
307 $28)=11.01$, $p<0.0001$; Tukey's multiple comparisons TuS vs. EYFP $p=0.0002$, NAcSh vs. EYFP
308 $p=0.0002$, NAcC vs. EYFP $p=0.004$).
309
310 Since VTA neurons are known to co-release glutamate in addition to dopamine[35,56,57], and knowing
311 that ventral striatum neurons express glutamatergic receptors, we next sought to isolate the
312 influence of the above effect (**Fig 4**) on DA versus glutamate. We crossed *VGluT2 fl/fl* mice with
313 mice expressing Cre recombinase in all cells expressing tyrosine hydroxylase (*TH-Cre*), the rate-
314 limiting enzyme upstream for DA synthesis. This approach ensures that *VGluT2* is lacking from
315 tyrosine hydroxylase expressing neurons, thus eliminating the possibility of glutamate co-release

316 from TH+ neurons. As above, we injected *VGluT2fl/fl* x *TH-Cre* mice with the same ChR2-
317 expressing virus or associated control virus unilaterally into the VTA and implanted an optical
318 fiber terminating over the TuS to drive terminal excitation. Since photostimulation in all three
319 ventral striatum subregions of ChR2-expressing mice in the prior experiment drove sniffing, here
320 we excluded the NAc groups for simplicity. As shown in **Supplementary Figure 6**,
321 photostimulation of DAergic terminals in *VGluT2fl/fl* x *TH-Cre* mice elicited sniffing with
322 comparable temporal dynamics, frequency, and probability as in DAT^{IRES}-*Cre* mice (**see Fig 4**) and
323 at greater amounts in *VGluT2fl/fl* x *TH-Cre* mice than in EYFP controls.
324
325 We next wanted to determine whether DA release in the ventral striatum serves to 'initiate'
326 sniffing, or if it further can persistently drive sniffing over extended time courses. To test this, in
327 the same ChR2-treated DAT^{IRES}-*Cre* mice as in **Figures 4B-G,** we delivered repeated presentations
328 of the 25Hz photostimulation for either 120ms, 1s, 2s, or 4s. We predicted that if DA initiates
329 sniffing we would see transiently-evoked sniffing across all stimulation durations, whereas if DA
330 drives sniffing, we would see the duration of sniffing bouts track the duration of the
331 photostimulation. As shown in **Figure 4H**, we found that the dynamics of the sniffing bout were
332 equivalent regardless of photostimulation duration. Indeed, in all three ChR2-treated groups,
333 photostimulation of DAergic terminals elicited a statistically similar frequency of sniffing (TuS
334 mixed-effects analysis; $F(1.78, 6.53)=0.94$ $p=0.426$; NAcSh rmANOVA $F(1.63, 4.89)=0.924$,
335 $p=0.436$; NAcC rmANOVA $F(1.93, 5.79)=0.24$, $p=0.789$), and similar percentage of time sniffing
336 (TuS mixed-effects analysis $F(1.18, 4.32)=1.57$, $p=0.284$; NAcSh rmANOVA $F(1.50, 4.5)=0.77$
337 $p=0.479$; NAcC rmANOVA $F(1.43, 4.30)=1.81$, $p=0.404$). These results indicate that DA release
338 into the ventral striatum initiates sniffing, but that it does not persistently drive a sniff bout.

339

340 Stimulation of respiratory brain stem regions known to support breathing can generate sniffing
341 patterns even in anesthetized mice (*e.g.* [15,16,58]). Is mesolimbic DA input to the ventral striatum
342 capable of initiating sniffing even in anesthetized mice? To test this, following the above
343 experiments, *DAT^{IRES}-Cre* mice injected with ChR2 were deeply anesthetized with urethane and
344 photostimulation was delivered. The baseline respiratory pattern and rate in these mice were both
345 stable and slow (<1.25Hz), indicating deep sedation. Breathing rate under anesthesia showed no
346 change upon photostimulation of DAergic terminals in either the TuS or the NAcSh and NAcC
347 (**Fig 5A - C**), suggesting that the VTA→ventral striatum DAergic circuit is a component of the
348 voluntary, not automatic, respiration-control system.

349

350 Sniffing bouts can be displayed in response to a variety of stimuli an animal may perceive in its
351 environment. While not well-studied, it is possible the temporal dynamics of sniffing bouts may
352 differ based upon what elicited the sniffing. We wanted to know if the sniffing bouts triggered by
353 DA release into the ventral striatum are similar, or distinct from, those which are elicited in
354 response to a stimulus or those bouts spontaneously generated. To address this, we used a machine
355 learning approach (**Fig 5D**). We converted 1s long sniffing traces (the 1s following bout onset)
356 into 1sec long instantaneous sniffing frequency arrays (10ms bin size). Next, we used K-nearest
357 neighbors with Diffusion Time Warping (DTW)[59–61] to calculate the difference in sniffing
358 frequency dynamics between frequency arrays. With DTW, the smaller the value reported in each
359 time bin corresponds to the dynamics between arrays being more similar at that moment. The
360 model was trained on DTW arrays from odor-evoked, spontaneously-generated, and
361 photostimulation-evoked data (n=63-70 arrays/group). Following, we fed the model DTW arrays

362 from each group to test how distinct the sniffing dynamics are between groups. In addition to using
363 the complete 'real' data set, we generated synthetic data using SMOTE (synthetic minority
364 oversampling technique[62]) to balance the sample numbers to 70 and separately, tested the model's
365 classification precision when providing it balanced samples of reduced numbers of 40 or 60 (**Fig**
366 **5E**). We found that photostimulation-evoked sniffing was highly distinct from all other types of
367 sniffing. In all runs, precision in classifying opto-evoked sniffing even exceeded the precision of
368 classifying odor-evoked sniffing, which is known to be highly stereotyped (**Figs 5Ei & 5Eii**). As
369 a comparison, spontaneously evoked sniffing was the most poorly classified, likely due to the
370 variability in these self-motivated bouts. While buzz-evoked sniffing was classified better than
371 spontaneous, the model struggled to classify it as well as opto-evoked sniffing. Both SMOTE and
372 the 60 sample runs yielded robust classification of photostimulation-evoked sniffing, with F1
373 scores (a single metric of model performance) of 0.9 in the 60-sample run, and 1.0 in the SMOTE
374 run. This result implies that DA release into the ventral striatum engages a distinct respiratory
375 pattern from that when an animal engages in self-motivated exploration or upon perception of an
376 environmental stimulus (*i.e.*, an odor).
377
378 As an additional experiment, we used an inhibitory optogenetic approach to suppress DAergic
379 terminals in either the NAcSh or the TuS to test whether this achieves reductions in sniffing. We
380 targeted these two ventral striatum subregions based upon their prominent elevations in DA upon
381 sniffing (**Figs 2 & 3**). We injected a Cre-dependent halorhodopsin (AAV5-EF1α-DIO-eNpHR 3.0-
382 EYFP) bilaterally into the VTA of *DAT^{IRES}-Cre* or *DAT^{IRES}-Cre x Ai9* mice (**Supplementary Fig**
383 **7**) and implanted bilateral 400µm diameter optical fibers terminating over the TuS or NAcSh (**Fig**
384 **6A & 6B**) to suppress terminal release of DA upon light stimulation. An example of a bilateral

385 cannula implant in the TuS is shown in **Figure 6C**. We sought to understand if suppressing
386 DAergic terminals could reduce sniffing both when mice spontaneously engage in sniffing, and
387 when mice sniff in response to a stimulus. To target spontaneous sniffing bouts, 5s long, 560nm
388 constant light stimulation was delivered through the optical fibers every 20s while mice were in
389 the plethysmograph. Since spontaneous bouts of sniffing can sometimes be short (~several
390 hundreds of milliseconds), we provided light every 20s without considering if the animal was
391 engaging in a sniff bout or not. We reasoned this would be a more objective stimulation paradigm
392 than if we were to trigger light off of every bout onset (*e.g.*, in a closed loop paradigm) which
393 could result in some 'learning' of the mouse to change its behavior.
394
395 As shown in the example in **Figure 6Di**, 560nm light stimulation suppressed sniffing frequency
396 during spontaneous events. Indeed, compared to control mice which received 5s long, 405nm
397 constant light stimulation (light stimulation unable to activate eNpHR[63]), photoinhibition of
398 DAergic terminals in the ventral striatum modestly suppressed respiratory frequency (**Fig 6Dii**; 2-
399 way rmANOVA, effect of light stimulation $F(1, 10)=11.08$, $p=0.0076$; Sidak's multiple
400 comparisons 560nm before light vs. during light $p=0.0037$). To test effects of DAergic inhibition
401 on stimulus-evoked sniffing, each mouse was presented with pseudorandom trials of odors,
402 including R(+)-limonene, thioglycolic acid, and peanut oil, each five times across a behavior
403 session. 560nm or 405nm light was delivered concurrently with odor and buzz delivery. For this
404 we used a longer light duration (7s, constant) to ensure that light was on upon the possible moment
405 the animal may perceive the stimulus and would typically engage in sniffing. Whereas inhibition
406 of DAergic terminals in the ventral striatum suppressed spontaneous sniffing (**Fig 4D**), there was
407 no effect of photoinhibition on the frequency of odor- or buzz-evoked sniffing in the TuS or NAcSh

408 (**Figs 6E & 6F**, two-way rmANOVA: NAcSh odor no effect of light $F(1, 4)=1.009$, $p=0.3719$;
409 NAcSh buzz no effect of light $F(1, 4)=1.117$, $p=0.3502$; TuS odor no effect of light $F(1, 5)=0.025$,
410 $p=0.8816$; TuS buzz no effect of light $F(1, 5)=4.696$, $p=0.083$). Taken together with the results of
411 the optical stimulation, these results cumulatively support that DA release in the ventral striatum
412 elicits sniffing.
413
414 ***Ventral striatum neural activity is associated with sniffing***
415 VTA DA is released onto spiny projection neurons in the ventral striatum expressing either the D1
416 or D2 DA receptor. Is the activity of these neurons associated with sniffing? To test this, we
417 performed two different experiments. First, we took advantage of an existing data set[64] wherein
418 extracellular neural activity was recorded from the TuS and respiration simultaneously sampled
419 from an intranasal cannula in behaving c57bl/6j mice throughout their engagement in an olfactory
420 discrimination task. In this task, mice were head-fixed which allowed for the snout to remain stable
421 for precision in the odor delivery. A subset of animals contributed respiratory data, and of them,
422 three mice also each contributed multiple single-units ($n=20$ total). As expected from head-fixed
423 animals[65,66], we observed bouts of sniffing in response to odor delivery and also during the inter-
424 trial interval separating odors (variable 15-17sec window). Further, as expected in head-fixed
425 animals and also seen in mice in the plethysmograph (*e.g.,* **Fig 3**), odor delivery significantly
426 increased the median of the instantaneous respiratory frequency (Wilcoxon rank-sum test, $z=-19.8$,
427 rank sum=$3.2\text{x}10^7$, $p<0.0001$, **Fig 7C**).
428
429 As shown in **Figures 7A & B**, we found that the firing of ventral striatum neurons occurs in
430 relation to both bouts of sniffing and even proximal to individual breaths which consisted of a

431 short duration respiratory cycle (*viz*., "sniffs"). Each of the neurons in this example displayed a
432 significant increase in firing in the 200ms following either a sniff or a sniff bout (**Fig 7B**; unit 1
433 $t(27)=5.44$, $p<0.0001$; unit 2 $t(27)=2.29$, $p=0.049$; unit 3 $t(27)=-3.46$, $p=0.001$). Looking across
434 the entire population of neurons, 19/20 (including the three from **Fig 7B**) were significantly
435 modulated relative to a short respiratory cycle ($p<0.05$, 2-tailed *t*-tests of firing rate 200ms before
436 vs. 200ms during sniffing across sniff occurrences). Among these, they were more likely to fire
437 within a short respiratory cycle during the inter-trial interval when the background respiratory rate
438 is slower (**Fig 7D**, mixed ANOVA, $F(3, 76)=31.48$, $p<0.0001$).
439
440 We then explored the relationship between the probability of a change in firing frequency relative
441 to either the first or last short duration breath in a bout of sniffing. To do this we identified
442 respiration cycles containing an 'initial spike' and three respiration cycles before and after that
443 initial spike. We observed that the initial spike occurs before the respiration cycle gets shorter (**Fig**
444 **7Ei**). This was especially the case during background breathing in the inter-trial interval when
445 breathing is slower, wherein cycles +1, 2, and 3 (relative to the initial spike) were significantly
446 higher in frequency than cycle 0 (ANOVA $F(6, 126)=6.37$, $p<0.0001$), while cycle 0 did not differ
447 from previous cycles. In the odor presentation period, however, although ANOVA analysis
448 showed there was a significant main effect of respiration cycles (ANOVA $F(6, 112)=4.43$,
449 $p=0.0005$), post hoc comparison showed that cycle 0 was not significantly different from the
450 adjacent cycles. Finally, we performed an additional analysis to determine if the last action
451 potential in a burst was "locked" to the cessation of a sniff bout. **Figure 7Eii** shows that there is
452 no change in respiration cycles aligned to the last spike, whether in the inter-trial interval or odor

453 presentation period. Thus, ventral striatum neural activity appears closely orchestrated with the
454 occurrence of sniffs.
455
456 As a second experiment to example the relationship between sniffing and recruitment of post-
457 synaptic ventral striatum neurons, we injected a Cre-dependent AAV expressing GCamP6f
458 (AAV.Syn.Flex.GCaMP6f.WPRE.SV40) into the TuS of D1-Cre and D2-Cre mice[67] which also
459 were subsequently implanted with a 400µm core optical fiber over the TuS (**Fig 8A & B**). An
460 extra-nasal flow sensor was positioned near the animal's nose to monitor sniffing[68]. This allowed
461 us to extend the results of the extracellular recordings (though they provided greatest temporal
462 resolution) by analyzing specifically D1 and D2 ventral striatum neuron activity across trials
463 wherein mice spontaneously entered into bouts of sniffing and also during odor-evoked sniffing.

464 Similar to that observed with DA release into the ventral striatum (**Fig 2**), the activity of both D1
465 and D2 neurons increased upon spontaneous sniffing bouts (**Fig 8C**). D1 and D2 neuron evoked
466 responses were comparable in their temporal dynamics, and both groups displayed similar evoked
467 frequency of sniffing (**Fig 8C**; unpaired $t(16)=1.084$, $p=0.294$). The activity of D2 neurons also
468 positively correlated with the frequency of spontaneous sniffing (**Fig 8Civ & 8Cv**) (D1 Pearson's
469 $r(37)=0.19$, $p=0.241$; D2 Pearson's $r(68)=0.48$, $p<0.0001$).

470 Novel odor delivery (*viz*., the first presentation of a given odor) evoked sniffing in both D1- and
471 D2-Cre mice (paired $t(11)=11.58$, $p<0.0001$), which habituated across subsequent presentations of
472 the same odor (**Fig 8Di**) (rmANOVA $F(1.73, 19.07)=35.82$, $p<0.0001$). During novel odor-evoked
473 sniffing bouts, D1 and D2 neurons increased in their activity (**Fig 8Dii & 8Div)**; D1-Cre: paired
474 $t(9)=7.03$, $p<0.0001$; D2-Cre: paired $t(9)=9.88$, $p<0.0001$). Reminiscent of changes in DA release
475 across repeated trials of odor-evoked sniffing (**Fig 3**), the activity of D1 and D2 neurons similarly

476 reduced across repeated presentations (**Fig 8Diii & 8Dv**; D1-Cre: rmANOVA $F(1.42, 12.77)=15.69$, $p=0.0008$; D2-Cre: rmANOVA $F(1.80, 16.21)=25.01$ $p<0.0001$). The evoked
477
478 neural activity and its subsequent adaptation across trials was similar in D1- and D2 mice (**Fig 8vi**;
479 two-way ANOVA, no effect of genotype $F(1, 18)=1.387$, $p=0.254$). These results indicate that the
480 activity of DA receptor-expressing ventral striatum neurons post-synaptic from midbrain DAergic
481 terminals is associated with sniffing.

482

483 ***DA receptor antagonism in the ventral striatum reduces both the occurrence and frequency of***
484 ***sniffing***

485 Ventral striatum neural activity can be influenced by a wealth of
486 neurotransmitters/neuromodulators arising from numerous bottom-up and top-down brain regions.
487 For instance, NAc activity is influenced not only by DA, but also by glutamatergic inputs from the
488 frontal cortex[69]. While the above results suggest that sniff-evoked changes in mesolimbic DA
489 influx to the ventral striatum engages postsynaptic neurons, those results still beg the question: is
490 DA binding to DA receptors on ventral striatum neurons needed for an animal to initiate sniffing?

491

492 We implanted c57bl/6j mice of both sexes with bilateral indwelling infusion cannulae into either
493 the NAcSh or TuS (**Fig 9A**). We focused on antagonism of DA receptors in the TuS and NAcSh
494 since it was within these regions wherein we found the strongest correlation between DA levels
495 and sniffing frequency (**Figs 3 & 4**). Since TuS and NAcSh neurons may express D1, D2, or D3
496 receptors[70–74], across days in a counter-balanced within subject's design, each mouse was
497 intracranially infused with SCH23390, raclopride, or PG01037 to selectively inhibit D1, D2, or
498 D3 receptors, respectively. The infusion occurred 10min prior to placing the mouse into the

499 plethysmograph for respiratory monitoring, wherein we measured both spontaneous and sensory-
500 evoked sniffing bouts (**Fig 9B)**. We analyzed for effects of D1, D2, and D3 antagonism on both
501 the number of sniff bouts and their frequency, displayed spontaneously and stimulus-evoked. DA
502 receptor antagonism has some known sedative effects[75], and notably, DA receptor antagonism had
503 some effect on baseline breathing, with specifically D2 receptor antagonism in the NAcSh
504 influencing breath frequency (Wilcoxon signed-rank test W=-279, p =0.012; **Supplementary Fig**
505 **3**).
506
507 We found that D1 receptor binding contributed to spontaneous sniffing in that D1 receptor
508 antagonism in the TuS reduced the number of spontaneous sniffing bouts (**Fig 9Ci;** two-way
509 ANOVA, main effect of treatment $F(1, 24)=12.62$, $p=0.002$; Sidak's multiple comparisons TuS
510 VEH vs. SCH $p=0.023$). D1 receptor binding also contributed to sensory-evoked sniffing in that
511 D1 receptor antagonism in the TuS reduced the number of buzz-evoked bouts (**Fig 9Ei**; two-way
512 ANOVA, main effect of treatment $F(1, 24)=4.30$, $p=0.049$; Sidak's multiple comparisons TuS
513 VEH vs. SCH $p=0.048$).
514
515 Likewise, we found that D2 receptor binding contributed to spontaneous sniffing in that D2
516 receptor antagonism in both the TuS and NAc reduced the number and frequency of spontaneous
517 sniffing bouts (**Fig 9Cii**; two-way rmANOVA, main effect of treatment $F(1, 24)=48.64$, $p<0.0001$;
518 Sidak's multiple comparisons TuS VEH vs. RAC $p<0.0001$, NAc VEH vs. RAC $p=0.002$). D2
519 receptor binding in the TuS and NAc also contributed to odor-evoked sniffing in that D2 receptor
520 antagonism reduced the number of sniffing bouts (**Fig 9Dii**; two-way rmANOVA, main effect of
521 treatment $F(1, 24)=31.26$, $p<0.0001$; Sidak's multiple comparisons TuS VEH vs. RAC $p<0.0001$,

522 NAc VEH vs. RAC p=0.017). In contrast, we saw no effect of D3 receptor inhibition on
523 spontaneous or odor-evoked sniffing in either the TuS or NAcSh (**Fig 9Ciii, 9Diii, 9Eiii**).
524
525 Interestingly, D2 antagonism in both the TuS and NAc not only reduced the number of odor-
526 evoked bouts displayed by mice, but in both regions, the odor-evoked bouts which were displayed
527 were reduced in frequency (**Supplementary Fig 8Bi & 8Bii**; D1 two-way rmANOVA main effect
528 of treatment $F(1, 24)=7.75$, p=0.010; Sidak's multiple comparisons TuS VEH vs. SCH p=0.228,
529 NAcSh VEH vs. SCH p=0.056; D2 two-way rmANOVA, main effect of treatment $F(1, 24)=96.64$,
530 $p<0.0001$; Sidak's multiple comparisons TuS VEH vs. RAC $p<0.0001$, NAcSh VEH vs. RAC
531 $p<0.0001$). This was not observed during spontaneous sniffing bouts or buzz-evoked sniffing bouts
532 pointing to a unique system which supports the frequency of odor-evoked sniffing compared to
533 spontaneous sniffing which was influenced solely in terms of the total number of bouts. Altogether,
534 these results confirm that mesolimbic DA initiates sniffing by its actions upon D1 and D2 receptors
535 in the TuS and NAcSh.
536
537 **Discussion**
538 DA appears to partake in numerous functions[33,34,76,77]. For instance, DA can influence the
539 perceived salience of stimuli wherein DA might make certain smells stand out more[39], making
540 them more noticeable during sniffing. DA might enhance our sensitivity to sensory stimuli,
541 including odors, allowing them to be better detected at low levels[78]. DA is also involved in arousal
542 and attention mechanisms wherein it could heighten our alertness and focus on sensory inputs,
543 including odors and other cues[79,80]. Indeed, DA supports cognitive functions in humans during
544 non-olfactory functions such as during gazing[81]. Further, DA is involved in synaptic plasticity and

545 learning from experiences and adapting to new information. When sniffing odors, DA release,
546 including upon ventral striatum neurons, could contribute to the brain's ability to form associations
547 and learn information[30]. Likewise, when we encounter pleasant or novel odors, DA release might
548 contribute to feelings of pleasure and satisfaction[53]. Indeed, DA is a key transmitter in the brain's
549 reward system and is connected to motivation and exploration[82], wherein it may influence our
550 motivation to sniff, encouraging us to explore and investigate different odor landscapes.
551 Furthermore, several lines of evidence have documented the orchestration of sniffing during
552 motivated behaviors and even upon anticipation of a reinforcer. These functions of DA stated, no
553 prior work has mechanistically linked DA with the highly conserved and ethologically-relevant
554 behavior of sniffing. Our results support a model wherein DA acts upon the ventral striatum,
555 specifically upon neurons with D1 and D2 receptors in the TuS and NAcSh, to initiate sniffing and
556 even increase the frequency of sniffing. This finding perhaps is analogous to the known role of
557 DA in guiding attention in other sensory modalities, including in humans[83,84] We predict the
558 promotion of sniffing by DA is an essential component linking the historic cooccurrence of
559 sniffing with motivated states.
560
561 Stimulus active sampling behaviors have a tight linkage to both the acquisition and processing of
562 environmental information, and these are modulated by ascending monoaminergic
563 neurotransmission. For instance, stimulation of the locus coeruleus in rats increases the
564 responsiveness of barrel cortex neurons to whisker deflection[85]. In zebra finches, auditory coding
565 in the finch auditory cortex homologue is modulated by norepinephrine[86]. Likewise, visual
566 processing in the lateral geniculate nucleus of cats is modulated by dopamine[87]. In terms of active
567 sampling behaviors and their regulation by monoaminergic transmission, rhythmic licking in mice

568 can be suppressed by DA D1 receptor antagonism in the motor cortex[88]. The rhythmic movement
569 of the vibrissae ("whisking") is perhaps the most well-studied in terms of its modulation by
570 monoaminergic inputs. Serotonergic input from the dorsal raphe nucleus, whose neurons fire
571 rhythmically within the whisking frequency bands, generates whisking in rats and whisking can
572 be diminished by serotonin receptor antagonism in the dorsal raphe[89]. Also, recent evidence
573 indicates that mesolimbic DA input to the NAc in mice promotes orofacial behaviors including
574 whisking[41]. Our results add to these prior studies by establishing a necessary and sufficient role
575 for mesolimbic DA in the initiation of sniffing behavior in that not only does photostimulation of
576 DAergic terminals initiate sniffing bouts, but also, blockade of DAergic receptors and optical
577 inhibition of DAergic terminals suppresses the normal occurrence of sniffing and its frequency. In
578 line with these results, VTA→ventral striatum DA may serve as a pathway to facilitate adaptive
579 sniffing to promote olfactory search behavior, and moreover may shape odor processing given the
580 regulation of odor coding and perception by the respiratory rhythm[90–92]. Given the extensive
581 innervation of the olfactory bulb by neuromodulatory systems, including norepinephrine, and the
582 presence of DAergic interneurons in the olfactory bulb, one might speculate that odor processing
583 and perception are resultant from a delicate balance of neuromodulators[93], which not only
584 recognize a novel odor, but also consequentially instruct novel motor patterns. The time-course of
585 stimulation-evoked sniffing we report herein supports that indeed DAergic release into the ventral
586 striatum may not be the initial driver of novel-odor evoked sniffing, which can be as fast as
587 ~100ms[94].
588
589 We found heterogeneity of DA release in ventral striatum subregions. Previous work from
590 Menegas and colleagues reported that DA is only released in the tail of the striatum upon novel

odor presentation (which likely would entail sniffing), with negligible changes in DA levels seen in the ventral striatum[32]. It is interesting to note that in their study, ventral striatum recordings were largely acquired from the NAcC, wherein we similarly did not see increases in DA levels. Furthermore, the results of Menegas and colleagues even suggest subtle reductions in DA levels, which agrees with our current findings from the NAcC. We expand upon this work by investigating DA dynamics across all three ventral striatal regions which include the NAcC, NAcSh, and TuS while animals sniff. Our findings are reminiscent of those monitoring DA release during other behaviors which has uncovered heterogeneous levels of DA in the NAcC versus NacSh in manners likely supported by differing VTA neural pathways innervating these subregions[43,44,95]. Here we found that in comparison to the increases in DA upon sniffing in both the TuS and NAcSh, that the NAcC experienced reductions in DA release (**Figs 2 & 3**). This implies that sniffing increases tonic firing of VTA DAergic neurons, or suppresses firing of DAergic neurons, in the NAcSh and TuS and NAcC, respectively. That optical excitation of the terminals in any of the regions equally initiates sniffing suggests that this is overriding changes in VTA neuron firing which give rise to DA dynamics in the ventral striatum and also hints that heterogeneity in subregion DA dynamics are not a byproduct of interregional differences in DA clearance (*e.g.,* by different kinetics or function of the dopamine transporter). It is tempting to speculate that different DA dynamics in these subregions might stem from unique inputs from areas that may signal salience or arousal which would synapse on VTA GABAergic neurons, including projections from the TuS and NAc themselves[95]. Furthermore, different DA neuron populations in the VTA display heterogenous responses to novelty vs. reward[32,80,96,97], which might stem from functional subtypes of DAergic neurons. It will be important to investigate the differing VTA neuron populations which may

underly these subregion-specific differences in DA dynamics in the ventral striatum during sniffing.

What 'type' of sniffing does mesolimbic DA initiate? The machine learning model trained on different experimenter classified sniffing patterns (**Fig 5D**) points to mesolimbic DA-evoked sniffing as its own type of sniffing, unique from that a mouse would self-motivate upon the desire to explore (spontaneous) and that evoked by a sensory stimulus (like an odor or buzz). So, what type is it? Sniffing is a dynamic behavior which can be displayed in unique manners based upon context. For instance, dogs sniff at lower frequencies when searching the air for odors than when searching on the ground wherein they elevate their sniffing rate[98]. Rats also display sniffing in a distinct frequency band when transitioning from sampling odors to anticipating a reinforcer in an instrumental task in manners which suggests sniffing reflects strategic 'modes' or states[5]. Our results are in-line with these prior works and suggest that mesolimbic DA-evoked sniffing reflects a unique sniffing mode. Several reports have established links between specific brain regions, and neurons within those brain regions, in regulating adaptive respiration, although the role of those regions does not appear to initiate sniffing as much as shape more specific respiratory parameters (*e.g.* [99]). Our results wherein we varied photostimulation of DAergic terminals uncovered that the duration of evoked-sniffing bouts did not increase with more prolonged optical stimulation (**Fig 4H**). Considering that VTA DAergic neurons fire in characteristic phasic manners[100,101], this suggests that DA release into the ventral striatum is more so to initiate and possibly elevate sniffing frequency than to maintain its tonic display.

635 There are a few caveats to this study we believe important to note. First, optogenetic stimulation
636 of DAergic terminals, while herein an effective means at robustly driving sniffing, is likely driving
637 DA release onto postsynaptic neurons in supraphysiological manners. While we selected a
638 stimulation paradigm established by others to be effective on TuS projecting VTA terminals, it is
639 nevertheless likely DA is released at higher than usual levels. Nevertheless, both our
640 pharmacological data (**Fig 9**) and our work wherein we removed *VGluT* from tyrosine hydroxylase
641 expressing neurons (**Supplementary Fig 6**) all agree that DA is contributing to the initiation of
642 sniffing. It is also possible that some behavioral effects from the photostimulation are due to
643 backpropagation of activity into the VTA itself. Again though, the pharmacological results indicate
644 DA input to the ventral striatum is important for sniffing. Second, while DA release into the ventral
645 striatum initiates sniffing, and while in several of our analyses, DA levels were correlated with
646 sniffing frequency, this was not always the case. For instance, for the buzz stimulus experiments,
647 large DA levels were found despite the mice only displaying modest frequencies of sniffing. This
648 corresponds with other studies which have reported DA release in response to a variety of salient
649 stimuli. Finally, while D2 receptors are enriched on spiny projection neurons in the TuS and NAc,
650 they also serve autoreceptor functions on VTA DAergic terminals, including those innervating
651 these regions. So, while we know local D1 antagonism suppressed sniffing, it is possible the effects
652 of D2 antagonism are due to contributions of antagonizing D2 receptors on both the VTA terminals
653 (which would enhance DA release) and on spiny projection neurons.
654
655 Antagonizing DAergic receptors versus inhibiting DAergic terminals resulted in different effects
656 upon respiration. Whereas pharmacological inhibition of TuS D1 receptors and NAc D1 and D2
657 receptors influenced specific occurrences of sniffing, including both spontaneous and stimulus-

658 evoked sniffing (**Fig 9**), optical inhibition of DAergic terminals only impacted spontaneous events
659 (**Fig 6**). We reason this may be due to a few possibilities. In our photoinhibition experiments, we
660 targeted the TuS and NAcSh separately. Given the transient and specific nature of the
661 photoinhibition paradigm, it is likely that the inhibition of DA release in the TuS could not override
662 the resultant effects of DA release in the NAcSh on sniffing, or *vice versa*, therefore resulting in
663 modest changes in respiration. Why then did we see robust effects when we pharmacologically
664 inhibited DA receptors in a single region (**Fig 9 & Supplementary Fig 8)**? We reason this may
665 be because a direct antagonist infusion would inhibit a great number of post-synaptic receptors,
666 and this coupled with potential influences of the antagonists on autoreceptor function and the
667 massive collateralization of spiny projection neurons upon each other would yield more dramatic
668 changes in the ability of the cells to act upon presynaptic DA.
669
670 A major question is how the receipt of DA upon spiny projection neurons might ultimately drive
671 changes in the respiratory rhythm. Both the TuS and NAc have outputs into downstream structures
672 important for homeostatic regulation/control and limbic function. Ventral striatum spiny
673 projection neurons also feedback upon the VTA in manners regulating DA release and this too
674 could support, even if just bisynaptically, modulation of respiratory central pattern generators
675 which are sensitive to dopamine[102,103]. Perhaps one clue may reside from our results wherein we
676 attempted to stimulate sniffing under anesthesia and found that DA release into the TuS or NAc is
677 incapable of initiating sniffing (**Fig 5A & B**). This suggests that the functional 'sniffing' output
678 from the ventral striatum is within a structure which can drive changes in breathing but not under
679 anesthesia. It is not uncommon for stimulation of some respiratory control centers to be incapable
680 of altering respiration under anesthesia[21,103]. For instance, the ventral striatum projects to

681 hypothalamic nuclei that are known to innervate respiratory control nuclei in the respiratory pons
682 and could support entrainment of breathing at sniffing frequencies. Interestingly, these
683 hypothalamic targets are also state dependent in that changes in breathing frequency do not occur
684 upon stimulation under anesthesia [21]. Thus, there seems to be somewhat of a paradox in that in
685 some respiratory structures, including the PreBötzinger complex, high frequency stimulation is
686 incapable of driving respiration at frequencies greater than 6Hz[104,105]. Identifying what
687 downstream circuits link the TuS and NAc to respiratory brain stem circuits to orchestrate sniffing
688 remains an important goal. Our results point to D1 and D2 ventral striatum neurons being part of
689 a feedforward/feedback loop between the basal ganglia and respiratory control regions with
690 DAergic VTA neurons being an intermediary circuit node. While the bio-sensor based fiber
691 photometry recordings we used to capture changes in DA and ventral striatum D1 and D2 neurons
692 suggest that these signals may at times lag the onset of a sniff bout, we did not correct for the lag
693 inherit in photometry recordings. Despite that, in several of the examples provided, DA levels
694 begin to rise immediately upon sniff bout onset (*e.g.*, **Fig 2Eii**). Further, the TuS single unit
695 recordings offered temporal dynamics which point to firing of at least some TuS neurons
696 immediately prior to the detectable increase in sniffing. This ultimately leads us to speculate that
697 a signal arrives at the ventral striatum (regarding a novel odor, or a change in environment or
698 internal state) which is ultimately routed through basal ganglia to initiate sniffing by means of
699 actions in the respiratory brainstem. At that point, DA is released by activation of VTA DAergic
700 neurons (perhaps as even modulated by ventral striatum input itself, e.g.,[106,107]), which then, based
701 on our results, would further drive ("invigorate") sniffing by its actions on those same ventral
702 striatum neurons. If future studies support this reciprocal DAergic loop model for sniffing,
703 naturally they would need to incorporate inputs/outputs to frontal cortices, hypothalamic

704 structures, motor cortex, and other regions integral for the plethora of behaviors and states which
705 might coincide with sniffing. While in many of our measures the frequency of sniffing positively
706 correlated with the peak magnitude of DA levels (*e.g.,* **Figs 2 & 3**), some instances of sniffing did
707 not co-occur with major rises in DA (*e.g.,* **Supplementary Fig 2 and also as shown in Figs 2Fii**
708 **& 2Gii**) and so it is likely multiple circuits are at play which link DA with sniffing.
709
710 In conclusion, we report evidence that mesolimbic DA input into the ventral striatum contributes
711 to the display of the widely conserved behavior of sniffing. The nature of sniffing being integral
712 to both olfaction and motivated behaviors implicates this circuit in a wide array of functions.
713 Especially in macrosmatic animals, like the mice studied herein, olfaction is crucial for appropriate
714 social behaviors, avoiding predation, and foraging. Based upon our evidence, we propose it is
715 likely this circuit provides a neuromodulatory means whereby motivated states signaled by DA
716 release tune the occurrence and frequency of sniffing in order for animals to thrive in the above
717 ethological scenarios.
718
719 **Methods**
720 *Animals*
721 Male and female mice were housed on a 12:12hr light-dark cycle with *ad libitum* access to food
722 and water. All behavioral testing took place during the light cycle. Mice with viral injections alone
723 were group housed (≤5 mice/cage) and any mouse with a chronic implant was single housed
724 following its surgical procedure. Food (Envigo Teklad Global, 18% rodent diet irradiated pellet,
725 Cat # 2018; Indianapolis, IN) and reverse osmosis water were available *ad libitum* except during
726 behavioral monitoring/recordings. Mice were housed in standard shoebox sized plastic cages

727 (Allentown Jag 75 micro-vent system; Allentown, PA; L: 29.2cm W: 18.5cm H:12.7cm) on a rack
728 made for individually vented cages. Corncob bedding and a Nestlet™ (Ancare; Bellmore, NY)
729 were in each cage along with manzanita sticks (Bio-Serve). Mice were housed on a 600-1800hr
730 light cycle with lights on during the daytime. Temperature in the room averaged 70 ± 2˚F, with
731 30-70% humidity and 10-15 room air changes per hour. The housing room was specific pathogen
732 free. Observation occurred from 1000-1700hrs. All animal care was conducted with in the
733 AAALAC animal research program of the University of Florida, in accordance with the guidelines
734 from the Guide for the Care and Use of Laboratory Animals and approved by the University of
735 Florida Institutional Animal Care and Use Committee.
736
737 Mouse lines included the following transgenic lines which all were maintained on a c57bl/6j
738 background (Jackson labs, strain #000664; RRID:IMSR_JAX:000664) and were bred in house
739 within a University of Florida vivarium. *drd1-Cre* and *drd-2-Cre* lines[67] were obtained from the
740 UC Davis Mutant Mouse Regional Resource Center (D1: EY262Gsat/Mmucd; D2: ER44Gsat).
741 *DAT^{IRES}-Cre* mice[108] (strain #006660; RRID: IMSR_JAX:006660), *TH-Cre* mice[109]; strain
742 #008601; RRID: IMSR_JAX:008601), *VGluT2 fl/fl mice*[110]; strain #012898; RRID:
743 IMSR_JAX:012898), and *Ai9* TdTomato Cre reporter mice[111] (strain # 007909,
744 IMSR_JAX:007909) were obtained from Jackson labs. A total of 178 mice (mixed sexes) were
745 used in this study for experimentation. Out of these, a total number of 51 were excluded from data
746 analyses due to experimental issues (*e.g.,* surgical complications, off-target brain implants, viral
747 injections which missed the target).
748

749 For all surgical procedures, under aseptic conditions, mice were anesthetized with Isoflurane (2-
750 4% in oxygen, IsoFlo®, Patterson Veterinary) and mounted in a stereotaxic frame where they were
751 maintained under Isoflurane. Body temperatures were maintained with a 38ºC heating pad
752 underneath. A local anesthetic, bupivacaine hydrochloride (Marcaine™, 5mg/kg subcutaneously,
753 s.c., Patterson Veterinary), and the analgesic meloxicam (5mg/kg, s.c., Patterson Veterinary) were
754 administered before incision and exposure of the skull. Mice receiving chronic implants (*e.g.,*
755 cannulae, optic fibers) were given meloxicam (0.5mg/kg, s.c.) for 3 days following surgery.
756
757 For viral injections, craniotomies were made over the ventral tegmental area (VTA) (-
758 3.6AP/0.35ML/-4.75DV), tubular striatum (TuS) (1.4AP/1ML/-4.90DV), nucleus accumbens
759 shell (NAcSh) (1.4AP/1ML/-4.40DV), and/or nucleus accumbens core (NAcC),(1.4AP/1ML/-
760 3.90DV) and a pulled glass micropipette containing the AAV was lowered into the region of
761 interest. Viruses were all delivered via the pulled pipette attached to a Nanoject III (Drummond
762 Scientific) at a rate of 2nl/s unless otherwise noted. After waiting 10min, the pipette was slowly
763 withdrawn from the brain. Unless followed by an implant in the same surgery, craniotomies were
764 sealed with dental wax, and the incision closed with wound clips.
765
766 For intranasal 'sniff' cannula implantation, a ~1mm diameter hole was drilled through the right
767 nasal bone, 1.5mm anterior the frontal/nasal fissure and 0.5mm lateral following prior methods [6].
768 A stainless-steel guide cannula (22GA, #C313G, P1 Technologies, Roanoke, VA) cut to extend
769 0.5mm below the pedestal was lowered through the craniotomy and secured with dental cement.
770 A dummy cannula (#C313DC, P1 Technologies, Roanoke, VA) cut to extend 0.2mm past the guide
771 cannula was also inserted when not recording from the mouse.

772

773 To record respiration, the dummy cannula was removed and a pressure transducer was connected
774 (CPXL04GF, Honeywell) to the cannula via a flexible piece of polyethylene tubing. The mouse
775 was then placed in the plethysmograph and recorded for 15min. Plethysmograph-recorded
776 transients were detected using a flow transducer (Data Sciences International) and digitized at
777 300Hz (0.1-12Hz band pass; Tucker Davis Technologies, Alachua, FL), following a 500x gain
778 amplification (Cyngus Technology Inc, Southport, NC). Intranasal pressure transients were
779 amplified and digitized using the same settings.

780

781 **Anatomical Tracing**

782 For synaptophysin injections, a craniotomy was made over the VTA, and a micropipette containing
783 100nL of pAAV-hSyn-FLEx-mGFP-2A-Synaptophysin-mRuby (Addgene 71760-AAV1; titer:
784 $9.8x10^{12}$vg/mL) was injected unilaterally into the VTA of *DAT*^{IRES}-*Cre* mice.

785

786 3 weeks following injections, mice were overdosed with sodium pentobarbital (Fatal-Plus,
787 Patterson Veterinary) and transcardially perfused with 0.9% saline followed by 10% phosphate-
788 buffered formalin. Brains were removed and stored in a 10% formalin in 30% sucrose solution at
789 4ºC prior to sectioning. Brains were coronally sectioned at 40µm and sections were stored in Tris-
790 buffered saline with 0.03% sodium azide.

791

792 *Image acquisition and quantification*

793 Brain regions of interest were identified using the mouse brain atlas[112]. For the TuS, 12 images
794 were acquired spanning 1.94mm - 0.14mm anterior to Bregma. For the nucleus accumbens, a total
795 of 8 images were acquired spanning 1.94mm – 0.74mm anterior Bregma.
796
797 Images were acquired with a Nikon Eclipse Ti2e fluorescent microscope. For brains with
798 synaptophysin injections (*n*=6 mice), images were acquired at 20x magnification across the
799 hemisphere ipsilateral to the injection site, and Z-stacked at every 4µm. For quantification, regions
800 of interest (ROIs) were drawn around areas of interest, namely the NAcC and NAcSh along with
801 the medial and lateral TuS. To determine the medial and lateral portions, the TuS was divided into
802 thirds and the most medial or lateral third was used to ensure distinctness between the two
803 regions[113]. Images were preprocessed to decrease average background fluorescence and enhance
804 contrast. A semiautomated counting algorithm created within NIS elements software (Nikon) was
805 used to detect and count fluorescent puncta, allowing for an unbiased estimation of puncta
806 numbers. Puncta were identified and quantified based on their size and fluorescence intensity via
807 bright-spot detection.
808
809 To reconstruct synaptophysin injection sites **(Supplementary Fig 1)**, the VTA was imaged from
810 -2.92 to -3.80mm posterior bregma, as identified with use of a brain atlas[112]. Next, an experimenter
811 (A. C.-L.) identified and marked GFP+ cell bodies in VTA schematics within Adobe Illustrator.
812
813 **Fiber photometric recording in the plethysmograph**
814 *Virus injection and optical fiber implant*

815 C57bl/6j mice were injected unilaterally in the NAcSh, NAcC, or TuS (*n*=7/group) with 100nL
816 pAAV.hSyn-GRAB_DA1h (Addgene 113050, titer: $1x10^{13}$vg/mL)[50]. For controls, c57bl/6j mice
817 were injected unilaterally in NAcSh, NAcC, or TuS (*n*=2-4/group) with 100nL pAAV.hSyn-
818 GRAB_DA-mut (Addgene 140555, titer: $1x10^{13}$ vg/mL). Viral injections were performed as
819 previously described (see 'Animals'). In the same surgery, a 400µm core, 0.48NA optical fiber
820 secured in a 2.5mm outer diameter metal ferrule was chronically implanted to terminate in the
821 TuS, NAcSh, or NAcC and affixed to the skull with dental cement. Animals were recorded from
822 3-5 weeks following surgery.
823
824 *Photometry*
825 465nm ($GRAB_{DA}$/$GRAB_{DA}$-mut excitation wavelength, driven at 210Hz) and 405nm (UV
826 excitation wavelength, driven at 330Hz; control) light emitting diodes (TDT, RZ10x) were coupled
827 to a fluorescent minicube (Doric lenses, FMC6) via 200µm, 0.22NA FCM optic fiber patch cords.
828 Both excitation and emission light were directed through a single 400µm, 0.57NA patch cord
829 connected to the animal by the implanted 2.5mm metal ferrule. Emission light was directed
830 through the mini cube and coupled to femtowatt photoreceivers to monitor GFP and UV signals
831 (TDT, RZ10x). The emission signals were low-pass filtered (6th order), pulse demodulated, and
832 digitized (1kHz) using a Tucker Davis Technologies processor (TDT). All parameters for imaging
833 and acquisition of photometry data were consistent across all groups.
834
835 *Respiratory data acquisition*
836 To simultaneously monitor photometry signals and respiration, mice were gently tethered to the
837 patch cord and placed in a whole-body plethysmograph (Data Sciences International, St. Paul,

838 MN). Respiratory transients were detected using a flow transducer (Data Sciences International)
839 and digitized at 300Hz (0.1-12Hz band pass; Tucker Davis Technologies, Alachua, FL), following
840 a 500x gain amplification (Cyngus Technology Inc, Southport, NC). Within all plethysmography
841 recordings, we analyzed the instantaneous frequencies of the peak-detected respiratory signal to
842 identify periods indicative of sniffing[6]. Since mice rapidly transition in and out of sniffing bouts [6],
843 we restricted our analyses to more stable/pronounced bouts versus short bouts by only defining a
844 sniff bout as the occurrence of sniffing ≥6Hz for ≥1s in duration. Further, in some instances, mice
845 continuously sniff for numerous seconds and then reengage in another bout shortly thereafter.
846 Since these may reflect periods of more generalized arousal versus spontaneous exploratory
847 behavior, we excluded sniff bouts occurring in proximity to these long (>10s) sniffing bouts. In a
848 subset of mice, an observer *post-hoc* monitored video (10Hz, 640x480 resolution) which was
849 recorded simultaneously with respiratory signal from the plethysmograph to validate that focusing
850 on >6Hz changes in respiration was indicative of 'active sampling' behaviors from the mouse
851 (including snout directed investigation and head-turning) and found 1:1 correspondence
852 supporting use of respiratory signals from the plethysmograph as suitable for detecting active
853 investigation (of course in this set-up we could not see minor facial, motor or vibrissal
854 movements).
855
856 *Behavioral monitoring*
857 Behavioral sessions lasted approximately 30min during which mice were presented with both
858 olfactory and non-olfactory stimuli. To allow for examination of spontaneous sniffing, we included
859 5min periods where no stimuli were presented at the beginning (0-5min), middle (12-17min), and
860 end (28-33min) of a session. Spontaneous bouts for analysis were identified between 2-5min, 14-

861 17min, and 30-33min to ensure that they were far removed from any stimuli presentations.
862 Between 5-12min, 2 trials of 4 different stimuli were pseudorandomly presented. The final 3 trials
863 of pseudorandom stimuli presentations occurred between 17-28min. Each stimulus was presented
864 for 2s with a 60s inter-trial interval.
865
866 *Stimulus delivery*
867 Odors R(+)-limonene and thioglycolic acid (Sigma-Aldrich, >97% purity), and that of peanut oil
868 (La Tourangelle®, Woodland, CA), were presented to mice via a custom air-dilution odor delivery
869 device connected to the plethysmograph (see Results for rationale in selecting these specific
870 odors). During experimentation, 2mL of all odors were contained in 40mL glass headspace vials
871 at room temperature. Computer-controlled and user-initiated openings of valves allowed for odors
872 to pass through headspace vials at a flow rate of 50mL/min, following which they were mixed with
873 a carrier stream of clean filtered room air delivered by a pump (1L/min; Tetra Whisper, Melle,
874 Germany) before being introduced into the plethysmograph. All odors were handled within
875 independent tubing to prevent cross-contamination. Following each odor presentation, odor-
876 vaporized air was passively cleared from the plethysmograph through an exhaust outlet at the
877 chamber's ceiling since the filtered room air is continuously delivered. Serving as a non-olfactory
878 stimulus, a vibration motor (3V, 12000 RPM; BestTong), referred to as "buzz," was secured to the
879 outside of the plethysmograph. During trials of pseudorandom stimulus presentations, each
880 stimulus was presented for 2s with a 60s inter-trial interval.
881
882 **Fiber photometric recording in head-fixed mice**
883 *Virus injection and optical fiber implant*

884 Mice for this method were also used for data collection and their results published (albeit from
885 different stimulus conditions wherein analyses were performed on well-learned odor-associated
886 pairs) in a prior study[40]. As we previously described in that study, *D1-Cre* and *D2-Cre* mice were
887 injected in the TuS with 1µL AAV5-EF1α-DIO-GCaMP6f-WPRE (obtained from the Penn Vector
888 Core in the Gene Therapy Program of the University of Pennsylvania, 5.43×10^{13}GC/mL). Viral
889 injections were performed as described above (see 'Animals'). Two weeks later, a 400µm core,
890 0.48NA optical fiber secured in a 2.5mm metal ferrule was chronically implanted to terminate in
891 the TuS. A plastic head-bar was also affixed to the skull with dental cement for later head fixation.
892 Animals were given a week for surgical recovery before undergoing behavioral testing.
893
894 *In vivo fiber photometry*
895 465nm (GCaMP excitation wavelength, driven at 210Hz) and 405nm (UV excitation wavelength,
896 driven at 330Hz; control) light emitting diodes were coupled to a 5 port minicube (Doric lenses,
897 FCM5) using 400µm, 0.48NA FCM optic fiber patch cords. Both excitation and emission light
898 were directed through a patch cord connected to the animal by the implanted 2.5mm metal ferrule.
899 Emission light was directed through the 5-port mini cube and coupled to femtowatt photoreceivers
900 to monitor GFP and UV signals. The data were then digitized and pulse demodulated at 1kHz
901 using a Tucker Davis Technologies processor (TDT). All parameters for imaging and acquisition
902 of photometry data were consistent across D1- and D2-Cre mice.
903
904 *Behavioral sessions*
905 Animals were head-fixed and presented with sets of 3 novel odors, 4 times each. To enhance each
906 animal's contribution to a more rigorous data set, animals were tested a second time at least 24hrs

907 later with sets of 3 different novel odors. Odors were delivered for 2s duration with a 17 ± 2s inter-
908 trial interval through an odor port positioned 1cm from the animal's snout.
909
910 *Stimulus delivery*
911 Odors were presented through an olfactometer and delivered through an odor port positioned 1cm
912 from the animal's snout. Odors included ethyl butyrate, 1,7-octadiene, isopentyl acetate, heptanal,
913 2-heptanone, R(+)-limonene, ethyl propionate, S(-)-limonene, methanol, methyl valerate, 2-
914 butanone, 1,4-cineole, butanal, propyl acetate, allylbenzene, allyl bromide, isobutyl propionate,
915 and 2-methylbutyraldehyde (Sigma Aldrich, all > 97% purity). Odors were diluted to 1Torr in
916 mineral oil and further diluted by mixing 100mL odor vaporized N_2 with 900mL medical grade
917 N_2 (Airgas). Stimuli were therefore presented at a total flow rate of 1L/min. Odor was continuously
918 flowing to the odor port but removed by a vacuum prior to reaching the animal. Odor sets used
919 varied across animals and across sessions.
920
921 *Respiratory data acquisition*
922 Respiration was recorded via an extranasal flow sensor (CPXL04GF, Honeywell) positioned near
923 the animal's nose as described[68]. A 1/8" inner diameter hose which terminated into the flow sensor
924 was placed ~7-10mm from the nose of the mouse during head fixation.
925
926 **Optogenetic stimulation in the plethysmograph**
927 *Virus injection and fiber implant*
928 *DAT^{IRES}-Cre x Ai9* mice or *VGluT2 fl/fl x TH-Cre* mice were injected unilaterally in the VTA with
929 400nL AAV5-EF1α-DIO-hChR2(E123T/T159C)-EYFP (Addgene 35509, titer: 1.3x10^{13}vg/mL)

930 or AAV5-EF1α-DIO-EYFP (for controls, UNC vector Core, titer: $3.5x10^{12}$vg/mL). While we used
931 *DAT* to drive Cre expression in DAergic neurons in other experiments in this study, here we used
932 the gene encoding tyrosine hydroxylase (*TH*) and specially *VGluT2 fl/fl x TH-Cre* mice since this
933 line was already available in-house. While this *TH*-based strategy may not had captured the
934 identical cell population as in the DAT-based strategy, and *VGluT2* may have been removed from
935 non-DA cells in the VTA[114], this mouse line allowed us to isolate the influence of DA on sniffing
936 from glutamate. Viral injections were performed as previously described. In the same surgery, a
937 300µm core 0.39 NA optical fiber in a ceramic ferrule was chronically implanted to terminate in
938 the TuS, NAcSh, or NAcC in *DAT^{IRES}-Cre x Ai9* mice or in the TuS for *VGluT2 fl/fl x TH-Cre* and
939 affixed to the skull with dental cement. Animals were tested no sooner than 4 weeks following
940 surgery.
941
942 To reconstruct ChR2.EYFP injection sites in the VTA of *DAT^{IRES}-Cre* mice (**Supplementary Fig**
943 **3**), the VTA was imaged from -2.92 to -3.80mm posterior bregma, as identified with use of a brain
944 atlas[112]. An independent rater used Adobe Illutrator to trace density of expression across images.
945
946 *Light stimulation and behavioral monitoring*
947 Optogenetic stimulation (25Hz, 15ms pulse width, 1s duration, 18mW[3]) was delivered by a 473nm
948 laser (CrystaLaser, DL473-100) and through a 300µm, 0.39NA fiber connected the laser to a fiber
949 optic rotary joint, with a 400µm, 0.47NA fiber connecting the rotary joint to the mouse (brass
950 mating sleeve). This paradigm was based on prior studies[39,40,54] and pilot work done in the lab.
951 Animals (*DAT^{IRES}-Cre*: TuS *n*=11, NAcSh *n*=6, NAcC *n*=6, EYFP controls *n*=9; *VGluT2 fl/fl x*
952 *TH-Cre*: TuS *n*=4, EYFP controls *n*=4) received one habituation day wherein they were gently

953 tethered to the path cable and placed in the plethysmograph for 20mins. The following day, animals
954 were again tethered, placed in the plethysmograph, and given a brief, 5min habituation period.
955 Following this, photostimulations (7-10/mouse) were delivered with a 2 ± 1min inter-trial interval.
956
957 A subset of *DAT*^{IRES}*-Cre* x *Ai9* (TuS: *n*=5, NAcSh: *n*=4, NAcC: *n*=4, EYFP controls: *n*=6)
958 underwent testing with varying durations of photostimulation. Stimulations at 25Hz with a 15ms
959 pulse width were delivered for durations of 120ms, 1s, 2s, or 4s. After a habituation day, mice
960 received a single stimulation parameter per day over four consecutive days. Each mouse underwent
961 the 1s duration on day 1, and the following 3 stimulation paradigms were randomized across mice
962 over the remaining 3 testing days. Photostimulations (9-11/mouse) were delivered with a 2 ± 1min
963 inter-trial interval.
964
965 Concluding testing, the same mice were then deeply anesthetized with urethane (1g/kg i.p.; Sigma
966 Life Science), tethered, and placed in the plethysmograph and photostimulated as described above.
967 Mice were transcardially perfused following recordings and within 30mins of urethane
968 administration.
969
970 **Optogenetic inhibition in the plethysmograph**
971 *Virus injection and fiber implant*
972 *DAT*^{IRES}*-Cre x Ai9* mice or *DAT*^{IRES}*-Cre* mice were injected bilaterally in the VTA with 300nL
973 AAV5-EF1α-DIO-eNpHR 3.0-EYFP (Addgene 26966, titer: 1.0x10^{13} GC/mL). Viral injections
974 were performed as previously described earlier in this study. In the same surgery, 400µm core,
975 0.39 NA optical fibers in ceramic ferrules were chronically implanted to bilaterally terminate in

976 the TuS or NAcSh and affixed to the skull with dental cement. To afford precision in the bilateral
977 spacing, the ferrules were first affixed in a 3D-printed adapter to ensure perfect 2.0mm from
978 epicenter-to-epicenter spacing (tip-to-tip). Animals were tested no sooner than 4 weeks following
979 surgery. Representative images of the primary injection site location of eNpHR 3.0-EYFP in the
980 VTA were confirmed and imaged by an independent experimenter (**Supplementary Fig 7**).
981
982 *Light stimulation and behavioral monitoring*
983 Optogenetic stimulation (7-9mW[3], 5-7s duration, constant, see Results for rationale) was delivered
984 by 405nm or 560nm LEDs (ThorLabs: Lx405 and Lx560). A 400µm, 0.48NA fiber connected the
985 LED to the mouse.
986
987 To examine whether optogenetic inhibition of DAergic terminals in the ventral striatum had any
988 effect on odor- or buzz-evoked sniffing, animals then underwent a similar behavioral session as
989 previously described (see Fiber photometric recording in the plethysmograph, Behavioral
990 monitoring**).** Animals first received one habituation day wherein they were gently tethered to the
991 path cable and placed in the plethysmograph for 20mins. Following this, in a counterbalanced,
992 within-subjects design, animals were tested over a 2-week period wherein they received concurrent
993 405nm or 560nm light delivery (7s duration, constant), initiated at the onset of both odor and buzz
994 delivery.
995
996 Separately, the same mice were again tested in a counterbalanced, within subject's design over 2
997 days. Behavioral sessions lasted ~10 minutes. Mice were gently tethered and placed in the

plethysmograph. Starting at minute 2, 5s (constant) of 405nm or 560nm light was delivered every 20s for 8 minutes, for a total of 24 light deliveries.

Machine learning to classify respiration

The study utilized a dataset comprising differently evoked sniffing data which consist of 261 samples, each 1s long. The dataset consisted of time series data representing respiratory frequencies (10ms bins).

Dynamic Time Warping (DTW) was employed as the distance metric for measuring the similarity between the time series data (respiratory frequency). DTW is known for its ability to align and compare time series data. DTW involves finding the optimal alignment between sets of data points of two sequences by warping the time axes. This allows the comparison of sequences with different lengths or different temporal structures. DTW creates a cost matrix, where each element represents the distance or dissimilarity between corresponding points in each of the two time series. Dynamic programming is used to efficiently find the optimal alignment by considering all possible alignments and selecting the one with the lowest cumulative distance [59]

The k-Nearest Neighbors (k-NN) algorithm was utilized for classification of unknown data points based on the majority class of its k-nearest neighbors in the feature space. In the context of time series data, DTW can be used as a distance metric in the k-NN algorithm instead of using traditional Euclidean distance. For a given query time series, the algorithm identifies the k-NN from the training set based on DTW distance[60]. For each query time series, the k-NN were identified and a majority voting scheme was employed to assign the class label.

1021

1022 Prior to applying the DTW k-NN algorithm, time series data were applied min-max normalization
1023 to ensure a uniform scale across all features. Subsequently, the dataset was divided into training
1024 and testing sets, with 80% of the samples allocated for training (208 samples) and 20% for testing
1025 (53 samples). The performance of the DTW k-NN algorithm was evaluated in terms of its
1026 accuracy, precision, recall, and F1-score. The max warping window was set at 7 and k at 3 which
1027 identified the combination that maximized the performance metrics during experiments.

1028

1029 The experiments were conducted using Google Colab (Google Brain Team, Mountain View,
1030 CA, USA). The DTW k-NN algorithm[61] was implemented in Python, utilizing the code available
1031 in the GitHub repository: https://github.com/markdregan/K-Nearest-Neighbors-with-Dynamic-
1032 Time-Warping. The dataset consisted of 63 photostimulation-evoked, 65 odor-evoked, 63 buzz-
1033 evoked, and 70 spontaneous respiratory/sniff bouts (*N*=261 total samples). SMOTE[62] was applied
1034 to generate synthetic data samples to bootstrap all groups to a total of 70 samples.

1035

1036 **Single unit recordings of ventral striatum neuron activity in head-fixed mice**

1037 These mice were used for data collection and their results published in a prior study from our
1038 group, with exception of any neural analyses aligned to intranasal respiration as done herein[64]. As
1039 we described in that study, c57bl/6j mice were implanted with eight-channel tungsten electrode
1040 arrays in the TuS and implanted with intranasal cannula for simultaneous respiratory monitoring.
1041 A plastic head-bar was also affixed to the skull with dental cement for later head-fixation. Animals
1042 were given a week for surgical recovery before undergoing behavioral testing wherein water-
1043 motivated mice were shaped to lick for a fluid reward for one odor, not a different one. Each animal

had 2-3 recording sessions on different days. Single neurons were sorted in Spike2, and then spiking and respiration were analyzed in MATLAB.

Units from the same animal but not from the same recording day were limited to different channels. The spontaneous period was within the intertrial interval excluding the five seconds from odor onset to avoid any swallowing or licking effect. The odor presentation period was defined as the time from odor onset to two seconds after odor onset. The respiration cycle was the interval between two positive peaks in respiration signals.

Sniffing burst detection

A high-pass filter (5 Hz) was applied to the respiration signal. The root mean square (RMS) was calculated using a 1s time window to quantify respiratory activity. The RMS was then transferred into the z-score. A threshold was set to 1 for sniffing onset detection.

Spike ratio and initial and terminal spike analyses

Respiration cycles were divided into four groups based on their duration, each containing 25% of the respiratory cycles. The spike number was then counted in each group for each unit. To establish control, 100 sets of randomly generated spikes were created, with the number of spikes in each set matching the actual spike number of the unit. The spike ratio was calculated as the spike number divided by the mean of the randomly generated spike number in each percentile group. The percentiles of the spontaneous and odor presentation periods were calculated separately. The initial spike was defined as the first spike without any spikes in the previous five respiration cycles.

1066 The terminal spike was the spike that had at least five spikes in the previous five respiration cycles
1067 and was not followed by any spikes in the five subsequent respiration cycles.
1068
1069 **Pharmacological manipulations**
1070 *Intracranial cannulae implantation*
1071 Bilateral craniotomies were made to target the the TuS and NAcSh. Stainless steel bilateral guide
1072 cannulae (26GA, 2.0mm center-to-center distance, 5.3mm long from the base of the pedestal, P1
1073 Technologies, Roanoke, VA) were lowered either to target the TuS (*n*=13) or the NAcSh (*n*=13).
1074 Cannulae were affixed to the skull via dental cement, and dummy cannulae with a 0.5mm
1075 projection from the end of the guide cannulae were then inserted and dust caps were added.
1076
1077 *Selective antagonists and intracranial infusions*
1078 SCH23390 (Tocris Bioscience, Bristol, UK) was dissolved in 0.9% sterile saline to a concentration
1079 of 0.5µg/µL. 0.1µL was infused to deliver 0.05µg/hemisphere. Raclopride (Tocris Bioscience,
1080 Bristol, UK) was dissolved in 0.9% saline + 5% dimethyl sulfoxide to a concentration of
1081 23.8µg/µL, and 0.21µL was infused to deliver 5µg/hemisphere. PG01037 (Tocris Bioscience,
1082 Bristol, UK) was dissolved in 0.9% saline + 12% DMSO to a concentration of 20µg/µL. 0.15µL
1083 was infused to achieve 3µg/hemisphere. Internal cannulae that were cut at lengths projecting
1084 0.5mm past the guide cannulae and thus terminating in the TuS or NAc were connected to 25GA
1085 polyurethane tubing (Instech Laboratories, Plymouth Meeting, PA) backfilled with dH2O. 1µL
1086 Hamilton syringes (Reno, NV) were used to inject total volumes ranging from 0.1-0.21µL. Mice
1087 were gently scruffed, dust caps and dummy cannulae were removed, and the internal cannulae was
1088 inserted before mice were placed back in their home cages for infusions. All drugs were infused

1089 at a rate of 0.1μL/min followed by a 2min rest period before the internal cannulae was removed,
1090 dummy cannulae and dustcap replaced. For all groups, behavioral testing began 10min following
1091 the start of drug infusion. All mice were tested across a 6 week period and recieved all selective
1092 antagonists and their corresponding vehicles, with 7 days between testing sessions.
1093
1094 *Behavioral methods*
1095 To monitor spontaneous and sensory-evoked sniffing behavior, mice were placed in the
1096 plethysmograph and underwent behavioral testing and stimulus delivery as previously described
1097 to monitor odor-, buzz-, and spontaneously-evoked sniffing (see Fiber photometric recording in
1098 the plethysmograph**,** Behavioral monitoring). Baseline breathing rates were identified as periods
1099 far removed from stimulation windows (*i.e.,* 2-5min, 14-17min, 30-33min).
1100
1101 **Histology**
1102 Mice receiving synaptophysin injections were perfused 3 weeks following injection. Mice
1103 undergoing behavior were perfused following the last day of behavioral monitoring. All mice were
1104 overdosed with sodium pentobarbital (Fatal-Plus, Patterson Veterinary) and transcardially
1105 perfused with 0.9% saline followed by 10% phosphate-buffered formalin. Brains were removed
1106 and stored (at 4ºC) in a 10% formalin in 30% sucrose solution prior to sectioning. Brains were
1107 coronally sectioned at 40μm and sections were stored in Tris-buffered saline with 0.03% sodium
1108 azide. Microscopic examination of tissue occurred on a Ti2e inverted fluorescent microscope, and
1109 only mice with on-target manipulations (cannulae locations, viral injections, viral injections +
1110 optic fiber placements) contributed to data sets. Verification of brain regions and target sites was
1111 aided by use of a brain atlas[112].

1112

1113 **Quantification and Statistical Analysis**

1114 *Analysis of respiratory data.*

1115 Inhalation peaks (sampled at 300Hz) were detected offline in Spike2 (Cambridge Electronic
1116 Design, Cambridge, UK). First, the respiratory data were filtered (0.1-12Hz band pass). Second,
1117 the maximum point of each respiratory cycle was identified, and instantaneous frequency was then
1118 calculated based off of the duration between one peak and its preceding peak. Data were down-
1119 sampled to 100Hz for subsequent analyses.

1120

1121 *Analysis of fiber photometry data.*

1122 Offline using a custom script in Spike 2, the GFP and UV signals were filtered (2nd order, 25Hz
1123 low pass) and smoothed with a sliding window (9 bins averaged). A first-degree polynomial fit
1124 was used to find the relationship between the signal and control channels and generate a scaled
1125 control channel. The fitted control channel was subtracted from the signal channel and z-scored
1126 $\Delta F/F$ traces were calculated using a 3s pre-event baseline window ($GRAB_{DA}$ analysis) or 2s pre-
1127 event baseline window (GCaMP6f for D1- and D2-Cre analysis).

1128

1129 Based on a series of pilot experiments, we found that on average, tethered animals in the
1130 plethysmograph typically do not perceive odors until 3s following odor control valve opening (as
1131 indicated by their reflexive/orienting sniffing responses). To account for this delay, the 3s after
1132 valve opening and odor onset serve as the pre-event baseline. Buzz-evoked $GRAB_{DA}$ signals were
1133 analyzed relative to the buzz onset, and spontaneous sniffing was analyzed relative to bout onset.

1134

1135 Peak $GRAB_{DA}$ signals and average sniff frequency were calculated within the 4s following odor
1136 analysis onset, 2s buzz duration, or spontaneous bout. Spontaneous sniffing bout durations varied
1137 and were identified based on prolonged periods of sniffing at frequencies ≥6Hz for ≥1s. Given the
1138 highly dynamic nature of sniffing and the rapid shift between respiratory frequencies in mice, we
1139 identified individual spontaneous sniff bouts wherein the mouse was sniffing at frequencies <6Hz
1140 for at least 2s prior to bout onset.
1141
1142 For D1- and D2-Cre GCaMP6f photometry, because animals were head-fixed and odor was
1143 delivered directly to the nose with high temporal precision, the 2s before odor delivery was used
1144 as the trial specific baseline for the z-scored ΔF/F values.
1145
1146 *Additional statistical methods*
1147 Data were analyzed in GraphPad Prism. All performed statistical tests were two-sided. Sample
1148 sizes are consistent with those reported in the field. All data are reported as mean ± SEM unless
1149 otherwise reported. Specific tests and *p* values used can be found in the Results section or the
1150 figure legends.

References

1. Wachowiak, M. All in a Sniff: Olfaction as a Model for Active Sensing. *Neuron* **71**, 962–973 (2011).
2. Uchida, N., Kepecs, A. & Mainen, Z. F. Seeing at a glance, smelling in a whiff: rapid forms of perceptual decision making. *Nat Rev Neurosci* **7**, 485–491 (2006).
3. Welker, W. I. Analysis of sniffing in the albino rat. *Behavior* **22**, 223–244 (1964).
4. Youngentob, S. L., Mozell, M. M., Sheehe, P. R. & Hornung, D. E. A quantitative analysis of sniffing strategies in rats performing odor discrimination tasks. *Physiol Behav* **41**, 59–69 (1987).
5. Kepecs, A., Uchida, N. & Mainen, Z. F. Rapid and precise control of sniffing during olfactory discrimination in rats. *J Neurophysiol* **98**, 205–213 (2007).
6. Wesson, D. W., Donahou, T. N., Johnson, M. O. & Wachowiak, M. Sniffing behavior of mice during performance in odor-guided tasks. *Chem Senses* **33**, 581–596 (2008).
7. Clarke, S. & Trowill, J. A. Sniffing and motivated behavior in the rat. *Physiol Behav* **6**, 49–52 (1971).
8. Isles, A. R., Baum, M. J., Ma, D., Keverne, E. B. & Allen, N. D. Urinary odour preferences in mice. *Nature* **409**, 783–784 (2001).
9. Ikemoto, S. & Panksepp, J. The relationship between self-stimulation and sniffing in rats: does a common brain system mediate these behaviors? *Behav Brain Res* **61**, 143–162 (1994).
10. Catania, K. C. Olfaction: Underwater 'sniffing' by semi-aquatic mammals. *Nature* **444**, 1024–1025 (2006).
11. Moberly, A. H. *et al.* Olfactory inputs modulate respiration-related rhythmic activity in the prefrontal cortex and freezing behavior. *Nat Commun* **9**, 1528 (2018).
12. Ashhad, S., Kam, K., Del Negro, C. A. & Feldman, J. L. Breathing Rhythm and Pattern and Their Influence on Emotion. *Annu Rev Neurosci* **45**, 223–247 (2022).
13. Moore, J. D. *et al.* Hierarchy of orofacial rhythms revealed through whisking and breathing. *Nature* **advance on**, (2013).
14. Kleinfeld, D., Deschênes, M. & Ulanovsky, N. Whisking, Sniffing, and the Hippocampal θ-Rhythm: A Tale of Two Oscillators. *PLoS Biology* vol. 14 Preprint at https://doi.org/10.1371/journal.pbio.1002385 (2016).
15. Ramirez, J.-M. & Baertsch, N. A. The Dynamic Basis of Respiratory Rhythm Generation: One Breath at a Time. *Annu Rev Neurosci* **41**, 475–499 (2018).
16. Del Negro, C. A., Funk, G. D. & Feldman, J. L. Breathing matters. *Nat Rev Neurosci* **19**, 351–367 (2018).
17. Moore, J. D. *et al.* Hierarchy of orofacial rhythms revealed through whisking and breathing. *Nature* **497**, 205–10 (2013).
18. Vann, N. C., Pham, F. D., Dorst, K. E. & Del Negro, C. A. Dbx1 Pre-Bötzinger Complex Interneurons Comprise the Core Inspiratory Oscillator for Breathing in Unanesthetized Adult Mice. *eNeuro* **5**, (2018).
19. de Sousa Abreu, R. P., Bondarenko, E. & Feldman, J. L. Phase- and state-dependent modulation of breathing pattern by preBötzinger complex somatostatin expressing neurons. *J Physiol* **600**, 143–165 (2022).
20. Oliveira, L. M., Baertsch, N. A., Moreira, T. S., Ramirez, J.-M. & Takakura, A. C. Unraveling the Mechanisms Underlying Irregularities in Inspiratory Rhythm Generation in a Mouse Model of Parkinson's Disease. *J Neurosci* **41**, 4732–4747 (2021).
21. Arthurs, J. W., Bowen, A. J., Palmiter, R. D. & Baertsch, N. A. Parabrachial tachykinin1-expressing neurons involved in state-dependent breathing control. *Nat Commun* **14**, 963 (2023).
22. Bhandare, A. *et al.* Analyzing the brainstem circuits for respiratory chemosensitivity in freely moving mice. *Elife* **11**, (2022).
23. Rosin, D. L., Chang, D. A. & Guyenet, P. G. Afferent and efferent connections of the rat retrotrapezoid nucleus. *J Comp Neurol* **499**, 64–89 (2006).

24. Bhandare, A. *et al.* Analyzing the brainstem circuits for respiratory chemosensitivity in freely moving mice. *Elife* **11**, (2022).
25. Rossi, J. & Panksepp, J. Analysis of the relationships between self-stimulation sniffing and brain-stimulation sniffing. *Physiol Behav* **51**, 805–813 (1992).
26. Mogenson, G., Jones, D. & Yim, C. From motivation to action: Functional interface between the limbic system and the motor system. *Prog Neurobiol* **14**, 69–97 (1980).
27. Haber, S. N. *Neuroanatomy of Reward: A View from the Ventral Striatum*. *Neurobiology of Sensation and Reward* (CRC Press, Boca Raton (FL), 2011).
28. Ikemoto, S. Dopamine reward circuitry: Two projection systems from the ventral midbrain to the nucleus accumbens-olfactory tubercle complex. *Brain Res Rev* **56**, 27–78 (2007).
29. Mingote, S. *et al.* Functional Connectome Analysis of Dopamine Neuron Glutamatergic Connections in Forebrain Regions. *Journal of Neuroscience* **35**, 16259–16271 (2015).
30. Wieland, S. *et al.* Phasic Dopamine Modifies Sensory-Driven Output of Striatal Neurons through Synaptic Plasticity. *The Journal of Neuroscience* **35**, 9946–9956 (2015).
31. Zahm, D. S. & Heimer, L. The ventral striatopallidothalamic projection. III. Striatal cells of the olfactory tubercle establish direct synaptic contact with ventral pallidal cells projecting to mediodorsal thalamus. *Brain Res* **404**, 327–331 (1987).
32. Menegas, W., Babayan, B. M., Uchida, N. & Watabe-Uchida, M. Opposite initialization to novel cues in dopamine signaling in ventral and posterior striatum in mice. *Elife* **6**, e21886 (2017).
33. Wise, R. A. Dopamine, learning and motivation. *Nat Rev Neurosci* **5**, 483–494 (2004).
34. Morales, M. & Margolis, E. B. Ventral tegmental area: cellular heterogeneity, connectivity and behaviour. *Nat Rev Neurosci* **18**, 73–85 (2017).
35. Stuber, G. D., Hnasko, T. S., Britt, J. P., Edwards, R. H. & Bonci, A. Dopaminergic Terminals in the Nucleus Accumbens But Not the Dorsal Striatum Corelease Glutamate. *Journal of Neuroscience* (2010) doi:10.1523/jneurosci.1754-10.2010.
36. Lobo, M. K. & Nestler, E. J. The Striatal Balancing Act in Drug Addiction: Distinct Roles of Direct and Indirect Pathway Medium Spiny Neurons. *Front Neuroanat* **5**, 41 (2011).
37. Phillips, P. E. M., Stuber, G. D., Heien, M. L. A. V, Wightman, R. M. & Carelli, R. M. Subsecond dopamine release promotes cocaine seeking. *Nature* **422**, 614–618 (2003).
38. Murata, K. *et al.* Opposing roles of dopamine receptor D1- and D2-expressing neurons in the anteromedial olfactory tubercle in acquisition of place preference in mice. *Front Behav Neurosci* **13**, (2019).
39. Zhang, Z. *et al.* Activation of the dopaminergic pathway from VTA to the medial olfactory tubercle generates odor-preference and reward. *Elife* **6**, e25423 (2017).
40. Gadziola, M. A. *et al.* A neural system for encoding the association of odors with rewarded outcomes and promoted behavioral engagement. *Cell Rep* **32**, 107919 (2020).
41. Li, W.-R. *et al.* Neural mechanisms underlying uninstructed orofacial movements during reward-based learning behaviors. *Current Biology* (2023) doi:10.1016/j.cub.2023.07.013.
42. Watabe-Uchida, M., Zhu, L., Ogawa, S. K., Vamanrao, A. & Uchida, N. Whole-Brain Mapping of Direct Inputs to Midbrain Dopamine Neurons. *Neuron* **74**, 858–873 (2012).
43. Beier, K. T. *et al.* Circuit Architecture of VTA Dopamine Neurons Revealed by Systematic Input-Output Mapping. *Cell* **162**, 622–634 (2015).
44. Badrinarayan, A. *et al.* Aversive Stimuli Differentially Modulate Real-Time Dopamine Transmission Dynamics within the Nucleus Accumbens Core and Shell. *The Journal of Neuroscience* **32**, 15779–15790 (2012).
45. Lammel, S., Ion, D. I., Roeper, J. & Malenka, R. C. Projection-Specific Modulation of Dopamine Neuron Synapses by Aversive and Rewarding Stimuli. *Neuron* **70**, 855–862 (2011).
46. Floresco, S. B. The Nucleus Accumbens: An Interface Between Cognition, Emotion, and Action. *Annu Rev Psychol* **66**, 25–52 (2015).
47. Wesson, D. W. The Tubular Striatum. *Journal of Neuroscience* **40**, 7379–7386 (2020).

48. Ikemoto, S. Involvement of the Olfactory Tubercle in Cocaine Reward: Intracranial Self-Administration Studies. *The Journal of neuroscience* **23**, 9305–9311 (2003).
49. Murata, K., Kanno, M., Ieki, N., Mori, K. & Yamaguchi, M. Mapping of Learned Odor-Induced Motivated Behaviors in the Mouse Olfactory Tubercle. *The Journal of Neuroscience* **35**, 10581–10599 (2015).
50. Sun, F. *et al.* A Genetically Encoded Fluorescent Sensor Enables Rapid and Specific Detection of Dopamine in Flies, Fish, and Mice. *Cell* **174**, 481-496.e19 (2018).
51. Mandairon, N., Poncelet, J., Bensafi, M. & Didier, A. Humans and Mice Express Similar Olfactory Preferences. *PLoS One* **4**, e4209 (2009).
52. Jagetia, S. *et al.* Inter- and intra-mouse variability in odor preferences revealed in an olfactory multiple-choice test. *Behavioral Neuroscience* **132**, 88–98 (2018).
53. Midroit, M. *et al.* Neural processing of the reward value of pleasant odorants. *Current Biology* **31**, 1592–1605 (2021).
54. Oettl, L.-L. *et al.* Phasic dopamine reinforces distinct striatal stimulus encoding in the olfactory tubercle driving dopaminergic reward prediction. *Nat Commun* **11**, 3460 (2020).
55. Gonzalez, L. S. *et al.* Ventral striatum dopamine release encodes unique properties of visual stimuli in mice. *Elife* **12**, (2023).
56. Sulzer, D. *et al.* Dopamine Neurons Make Glutamatergic Synapses in vitro. *The Journal of Neuroscience* **18**, 4588 LP – 4602 (1998).
57. Hnasko, T. S. *et al.* Vesicular glutamate transport promotes dopamine storage and glutamate corelease in vivo. *Neuron* **65**, 643–656 (2010).
58. Liu, S. *et al.* Divergent brainstem opioidergic pathways that coordinate breathing with pain and emotions. *Neuron* **110**, 857-873.e9 (2022).
59. Sakoe, H. & Chiba, S. Dynamic programming algorithm optimization for spoken word recognition. *IEEE Trans Acoust* **26**, 43–49 (1978).
60. Bagnall, A., Lines, J., Bostrom, A., Large, J. & Keogh, E. The great time series classification bake off: a review and experimental evaluation of recent algorithmic advances. *Data Min Knowl Discov* **31**, 606–660 (2017).
61. Regan, M. K-Nearest-Neighbors-with-Dynamic-Time-Warping. https://github.com/markdregan/K-Nearest-Neighbors-with-Dynamic-Time-Warping (2018).
62. Chawla, N. V, Bowyer, K. W., Hall, L. O. & Kegelmeyer, W. P. SMOTE: synthetic minority over-sampling technique. *J. Artif. Int. Res.* **16**, 321–357 (2002).
63. Zhang, F. *et al.* Multimodal fast optical interrogation of neural circuitry. *Nature* **446**, 633–639 (2007).
64. Gadziola, M. A., Tylicki, K. A., Christian, D. L. & Wesson, D. W. The Olfactory Tubercle Encodes Odor Valence in Behaving Mice. *The Journal of Neuroscience* **35**, 4515–4527 (2015).
65. Wesson, D. W., Verhagen, J. V & Wachowiak, M. Why Sniff Fast? The Relationship Between Sniff Frequency, Odor Discrimination, and Receptor Neuron Activation in the Rat. *J Neurophysiol* **101**, 1089–1102 (2009).
66. Verhagen, J. V, Wesson, D. W., Netoff, T. I., White, J. A. & Wachowiak, M. Sniffing controls an adaptive filter of sensory input to the olfactory bulb. *Nat Neurosci* **10**, 631–639 (2007).
67. Gong, S. *et al.* Targeting Cre Recombinase to Specific Neuron Populations with Bacterial Artificial Chromosome Constructs. *The Journal of Neuroscience* **27**, 9817 LP – 9823 (2007).
68. Jordan, R., Kollo, M. & Schaefer, A. T. Sniffing Fast: Paradoxical Effects on Odor Concentration Discrimination at the Levels of Olfactory Bulb Output and Behavior. *eNeuro* **5**, ENEURO.0148-18.2018 (2018).
69. Scofield, M. D. *et al.* The Nucleus Accumbens: Mechanisms of Addiction across Drug Classes Reflect the Importance of Glutamate Homeostasis. *Pharmacol Rev* **68**, 816–871 (2016).
70. Le Moine, C. & Bloch, B. D1 and D2 dopamine receptor gene expression in the rat striatum: Sensitive cRNA probes demonstrate prominent segregation of D1 and D2 mRNAS in distinct neuronal populations of the dorsal and ventral striatum. *J Comp Neurol* **355**, 418–426 (1995).

71. Mansour, A. *et al.* A comparison of D1 receptor binding and mRNA in rat brain using receptor autoradiographic and in situ hybridization techniques. *Neuroscience* **45**, 359–371 (1991).
72. Bouthenet, M. L. *et al.* Localization of dopamine D3 receptor mRNA in the rat brain using in situ hybridization histochemistry: comparison with dopamine D2 receptor mRNA. *Brain Res* **564**, 203–219 (1991).
73. Cepeda, C. *et al.* Differential electrophysiological properties of dopamine D1 and D2 receptor-containing striatal medium-sized spiny neurons. *European Journal of Neuroscience* **27**, 671–682 (2008).
74. Zhang, Y.-F. *et al.* Ventral striatal islands of Calleja neurons control grooming in mice. *Nat Neurosci* **24**, 1699–1710 (2021).
75. Starr, B. S. & Starr, M. S. Differential effects of dopamine D1 and D2 agonists and antagonists on velocity of movement, rearing and grooming in the mouse. Implications for the roles of D1 and D2 receptors. *Neuropharmacology* **25**, 455–463 (1986).
76. Markowitz, J. E. *et al.* Spontaneous behaviour is structured by reinforcement without explicit reward. *Nature* **614**, 108–117 (2023).
77. Berke, J. D. What does dopamine mean? *Nature Neuroscience* vol. 21 787–793 Preprint at https://doi.org/10.1038/s41593-018-0152-y (2018).
78. Ennis, M. *et al.* Dopamine D2 receptor-mediated presynaptic inhibition of olfactory nerve terminals. *J Neurophysiol* **86**, 2986–2997 (2001).
79. Nieoullon, A. Dopamine and the regulation of cognition and attention. *Prog Neurobiol* **67**, 53–83 (2002).
80. Bromberg-Martin, E. S., Matsumoto, M. & Hikosaka, O. Dopamine in Motivational Control: Rewarding, Aversive, and Alerting. *Neuron* **68**, 815–834 (2010).
81. Westbrook, A. *et al.* Dopamine promotes cognitive effort by biasing the benefits versus costs of cognitive work. *Science (1979)* **367**, 1362–1366 (2020).
82. Legault, M. & Wise, R. A. Novelty-evoked elevations of nucleus accumbens dopamine: Dependence on impulse flow from the ventral subiculum and glutamatergic neurotransmission in the ventral tegmental area. *European Journal of Neuroscience* **13**, 819–828 (2001).
83. Madras, B. K., Miller, G. M. & Fischman, A. J. The dopamine transporter and attention-deficit/hyperactivity disorder. *Biol Psychiatry* **57**, 1397–409 (2005).
84. Dang, L. C., O'Neil, J. P. & Jagust, W. J. Dopamine supports coupling of attention-related networks. *J Neurosci* **32**, 9582–7 (2012).
85. Motaghi, S., Sheibani, V., Farazifard, R. & Joneidi, H. Electrical stimulation of locus coeruleus strengthens the surround inhibition in layer V barrel cortex in rat. *Neurosci Lett* **401**, 280–284 (2006).
86. Lee, V., Pawlisch, B. A., Macedo-Lima, M. & Remage-Healey, L. Norepinephrine enhances song responsiveness and encoding in the auditory forebrain of male zebra finches. *J Neurophysiol* **119**, 209–220 (2018).
87. Zhao, Y., Kerscher, N., Eysel, U. & Funke, K. D1 and D2 receptor-mediated dopaminergic modulation of visual responses in cat dorsal lateral geniculate nucleus. *J Physiol* **539**, 223–238 (2002).
88. Chen, K., Vincis, R. & Fontanini, A. Disruption of Cortical Dopaminergic Modulation Impairs Preparatory Activity and Delays Licking Initiation. *Cerebral Cortex* **29**, 1802–1815 (2019).
89. Hattox, A., Li, Y. & Keller, A. Serotonin Regulates Rhythmic Whisking. *Neuron* **39**, 343–352 (2003).
90. Shusterman, R., Smear, M. C., Koulakov, A. A. & Rinberg, D. Precise olfactory responses tile the sniff cycle. *Nat Neurosci* **14**, 1039–1044 (2011).
91. Cury, K. M. & Uchida, N. Robust Odor Coding via Inhalation-Coupled Transient Activity in the Mammalian Olfactory Bulb. *Neuron* **68**, 570–585 (2010).
92. Iwata, R., Kiyonari, H. & Imai, T. Mechanosensory-Based Phase Coding of Odor Identity in the Olfactory Bulb. *Neuron* **96**, 1139-1152.e7 (2017).

93. Linster, C. & Cleland, T. A. Neuromodulation of olfactory transformations. *Curr Opin Neurobiol* **40**, 170–177 (2016).
94. Wesson, D. W., Carey, R. M., Verhagen, J. V & Wachowiak, M. Rapid encoding and perception of novel odors in the rat. *PLoS Biol* **6**, e82 (2008).
95. Yang, H. *et al.* Nucleus Accumbens Subnuclei Regulate Motivated Behavior via Direct Inhibition and Disinhibition of VTA Dopamine Subpopulations. *Neuron* **97**, 434-449.e4 (2018).
96. Tapper, A. R. & Molas, S. Midbrain circuits of novelty processing. *Neurobiol Learn Mem* **176**, 107323 (2020).
97. Azcorra, M. *et al.* Unique functional responses differentially map onto genetic subtypes of dopamine neurons. *Nat Neurosci* **26**, 1762–1774 (2023).
98. Steen, J. B., Mohus, I., Kvesetberg, T. K. & Walloe, L. Olfaction in bird dogs during hunting. *Acta. Physiol Scand* **157**, 115–119 (1996).
99. Angelakos, C. C. *et al.* A cluster of neuropeptide S neurons regulates breathing and arousal. *Current Biology* **33**, 5439-5455.e7 (2023).
100. Schultz, W., Dayan, P. & Montague, P. R. A Neural Substrate of Prediction and Reward. *Science (1979)* **275**, 1593–1599 (1997).
101. Grace, A. & Bunney, B. The control of firing pattern in nigral dopamine neurons: burst firing. *The Journal of Neuroscience* **4**, 2877–2890 (1984).
102. Sugita, T. *et al.* Breathing is affected by dopamine D2-like receptors in the basolateral amygdala. *Respir Physiol Neurobiol* **209**, 23–27 (2015).
103. Jhang, J., Liu, S., O'Keefe, D. D. & Han, S. A top-down slow breathing circuit that alleviates negative affect. *bioRxiv* (2023).
104. de Sousa Abreu, R. P., Bondarenko, E. & Feldman, J. L. Phase- and state-dependent modulation of breathing pattern by preBötzinger complex somatostatin expressing neurons. *J Physiol* **600**, 143–165 (2022).
105. Vann, N. C., Pham, F. D., Dorst, K. E. & Del Negro, C. A. Dbx1 Pre-Bötzinger Complex Interneurons Comprise the Core Inspiratory Oscillator for Breathing in Unanesthetized Adult Mice. *eNeuro* **5**, ENEURO.0130-18.2018 (2018).
106. Zhang, Y.-F. *et al.* Ventral striatal islands of Calleja neurons bidirectionally mediate depression-like behaviors in mice. *Nat Commun* **14**, 6887 (2023).
107. Edwards, N. J. *et al.* Circuit specificity in the inhibitory architecture of the VTA regulates cocaine-induced behavior. *Nat Neurosci* **20**, 438 (2017).
108. Bäckman, C. M. *et al.* Characterization of a mouse strain expressing Cre recombinase from the 3′ untranslated region of the dopamine transporter locus. *genesis* **44**, 383–390 (2006).
109. Savitt, J. M., Jang, S. S., Mu, W., Dawson, V. L. & Dawson, T. M. Bcl-x Is Required for Proper Development of the Mouse Substantia Nigra. *The Journal of Neuroscience* **25**, 6721–6728 (2005).
110. Tong, Q. *et al.* Synaptic Glutamate Release by Ventromedial Hypothalamic Neurons Is Part of the Neurocircuitry that Prevents Hypoglycemia. *Cell Metab* **5**, 383–393 (2007).
111. Madisen, L. *et al.* A robust and high-throughput Cre reporting and characterization system for the whole mouse brain. *Nat Neurosci* **13**, 133–140 (2010).
112. Paxinos, G. & Franklin, K. *The Mouse Brain in Stereotaxic Coordinates*. (Academic Press, San Diego, 2000).
113. Martin-Lopez, E., Xu, C., Liberia, T., Meller, S. J. & Greer, C. A. Embryonic and postnatal development of mouse olfactory tubercle. *Molecular and Cellular Neuroscience* **11**, 82–96 (2019).
114. Lammel, S. *et al.* Diversity of Transgenic Mouse Models for Selective Targeting of Midbrain Dopamine Neurons. *Neuron* **85**, 429–438 (2015).

Acknowledgements:

We thank Jacqueline Sipio for help with histology and Ellyse Thomas for expert animal care assistance.

This work was supported by R01DC014443 and R01DC016519 to D.W.W., R01DA049545, R01DA049449 and R01NS117061 to D.W.W. and M.M., R01DC006213 to M.M., and R00HL159232 to A.G.V.. N.L.J. was supported by NIDCD T32015994 and F31DC020364.

Author Contributions:

Conceptualization: NLJ & DWW
Methodology: NLJ, ACL, LAS, AGV, UMA, ZZ, MAG
Investigation: NLJ, ACL, LAS, ZZ, UMA, MAG
Visualization: NLJ, DWW, ACL
Funding acquisition: NLJ, DWW, MM, AGV
Supervision: DWW
Writing – original draft: NLJ
Writing – review & editing: NLJ, DWW, AGV, MM, UMA, LAS, ACL, ZZ

Competing interests: Authors declare that they have no competing interests.

Figures & Legends

Figure 1. Organization of midbrain dopamine input into the tubular striatum and nucleus accumbens. A. Schematic of tracing paradigm. *DAT^{IRES} -Cre* mice were injected into their VTA with AAV.FLEX.hSyn.mGFP.synaptophysin.mRuby allowing for mGFP expression in DAT+ cell bodies and synaptophysin.mRuby+ puncta in the terminals of DAT+ cells. Approximately 3 weeks later, coronal sections throughout the ventral striatum were collected for later fluorescence imaging and quantification of synaptophysin.mRuby+ puncta. **B.** Example of synaptophysin.mRuby expression throughout the ventral striatum, with key regions of interest outlined by dashed lines. **C.** Quantification of synaptophysin+ puncta throughout the anterior-posterior spans of regions of interest (n=6 mice). Data [puncta #'s/mm^2] are represented as mean ± SEM. Data smoothed for visualization purposes only. **D.** Histograms representing data in (**C**) with regions of interest segregated into their most anterior and posterior aspects (anterior most half vs. posterior most half). Data are mean ± SEM, points = individual mice. *p<0.5. abbreviations: VTA (ventral tegmental area), NAcSh (nucleus accumbens shell), NAcC (nucleus accumbens core), mTuS (medial aspect of the tubular striatum), LatTuS (lateral aspect of the tubular striatum), PCX (piriform cortex). (the anterior or posterior-most 200µm were used for quantification of these regions).

Figure 2. Self-motivated spontaneous sniffing is associated with DA levels. A. Diagram of the setup for simultaneous measurement of respiration by means of both whole-body plethysmography and an intranasal pressure cannula. Three mice were implanted with a cannula in its dorsal nasal recess and placed in the plethysmograph. Intranasal pressure changes were monitored by a pressure sensor connected to the cannula by a flexible tube passed through a fitted plug at the top of the plethysmograph and compared to whole-body changes. Image made with BioRender. **Bi**. Overlaid representative respiratory traces acquired from the plethysmograph (black) and intranasal cannula (blue) from an awake mouse. An example of high frequency sniffing is shown zoomed in and the expanded inset shows fidelity between the whole-body pressure and intranasal pressure signal. **Bii.** Example of the latency difference between respiratory peaks recorded by intranasal pressure and plethysmograph pressure during a high frequency sniffing bout with detected respiratory events (n=125 respiratory cycles). Overlaid respiratory traces (top) shows an intranasal pressure peaks aligned to time 0, and a plethysmograph pressure peak detected <60ms later. **Biii**. Histograms comparing respiratory frequencies measured from the plethysmograph and intranasal cannula. The plethysmograph reliably detected sniffing at both low and high respiratory frequencies with >99% accuracy (out of 3,239 respiratory events collected from 3 mice). **C.** Schematic of fiber photometry and plethysmograph system used to simultaneously record GRAB$_{DA}$ signals and sniffing behavior in unrestrained mice. Animals were injected with AAV.hSyn-GRAB_DA1h and implanted with an optic fiber in the TuS, NAcSh, or NAcC. 3-5 weeks later, animals were placed in the plethysmograph and 465nm and 405nm light were passed through dichroic mirrors before reaching the animal via patch cable and implanted optical fiber. GRAB$_{DA}$ and UV emissions were amplified by photoreceivers before being digitized along with simultaneous respiratory data. Image made with BioRender. **D.** Optic fiber implant locations in the TuS, NAcSh, and NAcC (n=7 mice/group). Within each region, ellipse color corresponds to same colored data in **Figures 2F-H and 3C-H**. **E.** Example of raw 465nm GRAB$_{DA}$ (green) and 405nm UV (purple) signals recorded in the TuS during a spontaneous sniff bout. Raw respiratory trace (resp) is shown below with interpolated instantaneous frequency above (Inst Hz- black trace). Sniff duration is indicated by the grey shaded

box. **Fi.** Averaged z-scored ΔF/F traces show an increase in $GRAB_{DA}$ levels in TuS during spontaneous sniff bouts. Average bout duration indicated by overlaid box plot. **Fii**. Significant positive correlation between $GRAB_{DA}$ levels in the TuS (the peak z-score during a spontaneous sniff bout) and average sniff frequency during bout (r=0.29, p=0.008). **Gi**. Averaged z-scored ΔF/F traces similarly show an increase in $GRAB_{DA}$ levels in the NAcSh during spontaneous sniff bouts. Average bout duration indicated by overlaid box plot. **Gii**. There was no correlation between $GRAB_{DA}$ levels in the NAcSh during spontaneous bout and sniffing frequency (r=0.12, p=0.249). **Hi**. Conversely, averaged z-scored ΔF/F traces show a decrease in $GRAB_{DA}$ levels in the NAcC during spontaneous sniff bouts. Average bout duration indicated by overlaid box plot. **Hii**. There was no significant correlation between $GRAB_{DA}$ levels in the NAcC during spontaneous bout and sniffing frequency (r=0.038, p=0.703). Abbreviations: resp (respiratory trace), Inst Hz (instantaneous frequency). Data in (Fi), (Gi), and (Hi) smoothed for visualization purposes only.

Figure 3. Bidirectional dopamine dynamics upon sensory-driven sniffing. A. Schematic of fiber photometry and plethysmograph system used to simultaneously record $GRAB_{DA}$ signals in the TuS, NAcSh, and NAcC and sniffing behavior in unrestrained mice (n=7/group) as used in Fig 2. Additionally, an olfactometer was used to deliver odors to animals in the plethysmograph, and a vibration motor (buzz) was attached to the outside of the plethysmograph. Image made with BioRender. **B.** Example of raw 465nm $GRAB_{DA}$ (green) and 405nm UV (purple) signals recorded in the TuS during an odor-evoked bout. Raw respiratory trace (resp) is shown below with interpolated instantaneous frequency above (Inst Hz- black trace). Grey shaded box denotes odor analysis window, starting 3 seconds following odor onset to account for the delay of odor delivery to the plethysmograph. **C-E.** Odor-evoked sniffing behavior and $GRAB_{DA}$ signals from mice with injections and optic ferrule implants in the TuS (C), NACSh (D), and NAcC (E). Average instantaneous sniffing frequency of TuS (Ci), NAcSh (Di), and NAcC (Ei) implanted mice across repeated odor presentations. Mean shown in black with individual mouse data across trials shown in light grey. Averaged z-scored ΔF/F across all 5 odor presentations in the TuS (Cii), NAcSh (Dii), and NAcC (Eii). Averaged peak of the z-scored $GRAB_{DA}$ response across trials in the TuS (Ciii), NAcSh (Diii), and NAcC (Eiii). Mean shown in black with individual mouse data across trials color coded to ellipse colors shown in **Figure 2D**. Significant positive correlations between $GRAB_{DA}$ levels (peak z-score during odor-evoked activity) and average sniff frequency during bout in the TuS, (r=0.65, p<0.0001, Civ) and NAcSh (r=0.51, p=0.002, Div) but not in the NAcC (r=-0.14, p=0.414, Eiv). **F-H.** Buzz-evoked sniffing behavior and $GRAB_{DA}$ signals from same mice with injections and implants in the TuS (F), NAcSh (G), and NAcC (H). Average instantaneous sniffing frequency of TuS (Fi), NAcSh (Gi), and NAcC (Hi) implanted mice across repeated odor presentations. Mean shown in black with individual mouse data across trials shown in light grey. Averaged z-scored ΔF/F across all 5 odor presentations in the TuS (Fii), NAcSh (Gii), and NAcC (Hii). Horizontal line depicts 2s buzz duration. Averaged peak of the z-scored $GRAB_{DA}$ response across trials in the TuS (Fiii), NAcSh (Giii), and NAcC (Hiii). Mean shown in black with individual mouse data across trials color coded to ellipse colors shown in **Figure 2D**. Significant positive correlation between $GRAB_{DA}$ levels and sniffing frequency in the TuS, (r=0.43, p=0.011, Fiv), but not the NAcSh (during buzz: r=-0.17, p=0.316; upon buzz offset: r=-0.074, p=0.673, Giv) or NAcC (r=-0.22, p=0.194, Hiv). **I.** Comparison of the peak-evoked $GRAB_{DA}$ responses across the TuS, NAcSh, and NAcC during odor-, buzz-, and spontaneously-evoked sniffing. Data are represented as mean ± SEM. Points = individual mice. ****p<0.0001,

***p<0.001, **p<0.01. Data shown in (Cii), (Dii), (Eii), (Fii), (Gii), and (Hii) are smoothed for visualization purposes only.

Figure 4. Initiation of sniffing by dopamine release into the ventral striatum. A. Schematic of optogenetically-evoked sniffing paradigm. *DAT^{IRES}-Cre x Ai9* mice were injected with AAV-EF1α-DIO-hChR2(E123T/T159C)-EYFP in the VTA, and optic fibers terminating in the TuS, NAcSh or NAcC were implanted in the same surgery. Control mice were injected with AAV-Ef1α-DIO-EYFP. At least 4 weeks later, mice were tethered and placed in the plethsymograph to optogenetically stimulate DA terminal release while monitoring sniffing. Image (right) made with BioRender. **B.** Optic fiber implant locations in the TuS, NAcSh, and NAcC (n=6-11 mice/group). **C.** Example respiratory data from a TuS implanted mouse across 10 trials of light stimulation. Timing of the 1s long, 25Hz photostimulation depicted by grey shaded box and dotted blue horizontal line. Raw respiratory traces are shown on the left, and corresponding instantaneous frequency for each trial shown in 2-dimensional histograms on the right. Dotted white line in 2-dimenional histogram depicts stimulation onset. **D**. 2-dimensional histograms across all mice tested within each group, showing individual trial data within mice. Example data from (C) denoted by the white star. Separation between mice marked by dark blue line. Stimulation onset is denoted by the vertical dotted white line, and 1s, 25Hz stimulation shown by the dotted blue trace. **E.** Mean sniffing frequency ± SEM during photostimulation across 10 trials in each group. **F.** Averaged z-scored respiratory frequency ± SEM of photostimulation-evoked sniffing. Stimulation onset denoted by vertical dotted black line and 25Hz, 1s duration by horizontal blue line. Group color legend matches what is shown in (E). **G**. Parameters of optogenetically-evoked sniffing during 1s photostimulation. All data presented as mean ± SEM, points = individual mice. ****p<0.0001, ***p<0.001, **p<0.01. **Gi.** Mean latency to sniff across groups. Animals that failed to reach 6Hz on >40% of trials were excluded from the EYFP control group. **Gii**. Mean percentage of time spent sniffing across groups. **Giii.** Max sniffing frequency reached during photostimulation. **Giv**. Mean probability that photostimulation will evoke sniffing. **H.** Averaged z-scored respiratory frequency during different photostimulation durations (100ms, 1s, 2s, 4s) compared to responses of EYFP controls stimulated for 1s in the TuS (Hi), NAcSh (Hii), and NAcC (Hiii). Insets in each panel show the percentage of time across all groups, calculated in a 4s window, that mice spend sniffing upon photostimulation.

Figure 5. State-dependence of a unique dopamine-evoked sniffing pattern. A. Example respiratory behavior of a TuS implanted mouse under urethane anesthesia. Raw respiratory traces (left) and corresponding 2-dimensional histogram (right) across 10 trials of photostimulation. 1s long, 25Hz photostimulation duration depicted by grey shaded box and dotted blue horizontal line. Dotted white line in the 2-dimensional histogram = photostimulation onset **B.** 2-dimensional histograms across 5 representative mice per group showing individual trial data within mice. Starred data represents example data from (A). Separation between mice denoted by dark blue line. Stimulation onset is denoted by the vertical dotted white line, and 1s, 25Hz stimulation shown by the dotted blue trace. Color scale matches that of **Figures 4C and D**. Little to no change in coloring highlights the substantial lack of any modulation in breathing rate under anesthesia. **C.** Averaged z-scored respiratory frequency of photostimulation-evoked sniffing. Stimulation onset denoted by vertical dotted black line and duration by horizontal blue dotted line. Inset shows the evoked z-scored average across all groups during light stimulation. **D.** Overview of machine learning applied to respiratory traces starting with dynamic time warping (DTW) between a 1s

odor-evoked sniff bout and 1s opto-evoked sniff bout. Bin size=10ms. 1s-long respiratory traces (100Hz) were converted to instantaneous frequency traces (also 1s long) and subjected to DTW to assess distance in proximal time-points. Subsequently, a model was trained on experimenter-identified traces from either buzz-, odor-, spontaneous-, or photostimulation-evoked respiration that were also previously subjected to DTW (see Methods). **Ei.** F1 score (single metric of model performance) for sniff types based on number of samples used per class. SMOTE=70 samples. **Eii.** Confusion matrix from SMOTE analyzed data displaying the classifier accuracy in predicting optogenetic-, odor-, buzz-, or spontaneously-evoked sniffing bouts. Classifier was trained on 80% of samples and tested on remaining 20%.

Figure 6. Inhibition of DA release into the ventral striatum and sniffing. A. Schematic of optogenetically-inhibited sniffing paradigm. *DAT^{IRES}-Cre* and *DAT^{IRES}-Cre x Ai9* mice were injected with AAV-EF1α-DIO-eNpHR 3.0-EYFP bilaterally in the VTA, and bilateral optic fibers terminating the TuS or NAcSh were implanted in the same surgery. At least 4 weeks later, mice were tethered and placed in the plethysmograph to optogenetically inhibit DA terminal release while monitoring sniffing. 560nm light was used to activate eNpHR and 405nm light was used for controls. Image (right) made with BioRender. **B.** Bilateral optic fiber implant locations in the TuS and NAcSh (*n*=5-6/group). **C.** Representative bilateral implant in the TuS. **Di.** Example of respiration during photoinhibition periods. Raw respiratory trace (resp) is shown with interpolated instantaneous frequency above (Inst Hz). 560nm LED duration indicated by red shaded box. **Dii.** Normalized respiratory frequency during the 3s before light stimulation compared to respiratory frequency during 5s light stimulation (405nm stimulation – left, 560nm stimulation – right). Blue dots indicate TuS implanted mice, green dots indicate NAcSh implanted mice. $^{**}p<0.01$. **E.** Average instantaneous sniffing frequency of TuS (Ei) and NAcSh (Eii) implanted mice across repeated odor presentations with concurrent delivery of 560nm or 405nm light. Mean during 560nm concurrent light delivery shown in red, with individual mouse data across trials shown in light red. Mean during 405nm concurrent light delivery shown in gray, with individual mouse data across trials shown in light grey. **F.** Average instantaneous sniffing frequency of TuS (Fi) and NacSh (Fii) implanted mice across repeated buzz presentations with concurrent delivery of 560nm (red) or 405nm (gray) light.

Fig. 7. Ventral striatum neuron activity is coupled with sniffing. Ai. Continuous recording of intranasal respiration (blue, inhale = upward deflection) along with single-unit activity from three units in the TuS. Grey shaded boxes indicate periods wherein non-novel odors were delivered. **Aii** is a magnified inset to help illustrate the temporal relationship between the three units in **Ai** and sniffing. **B.** Overdrawn waveforms and raster plots of spiking aligned to sniffing onset from the three units in **A** to illustrate that spiking often occurred following sniffing onset. **C.** Distribution of respiratory frequencies from the mice (*n*=3) during both spontaneous and odor-delivery periods (see Methods). **D.** Spike ratio histogram showing that more spiking occurs (*n*=20 units, across 3 mice) during higher frequency respiration than lower frequency respiration, and that this was greater when animals spontaneously transitioned into sniffing during the inter-trial interval than when sniffing during an odor – likely because the different basal respiratory rates in those states (as shown in **C**). **Ei** and **Eii.** Histograms of the firing frequency of the units in D, relative to either the first spike or final spike (Ei or Eii, respectively) indicating that the first

spike is predictive that the subsequent breath frequencies will be faster than the breaths prior to the first spike. *** = (ANOVA $F(6, 112)=4.43$, $p=0.0005$; see Results).

Figure 8. Sniffing is associated with recruitment of D1 and D2 spiny projection neurons. A. Schematic of the fiber photometry system for use in head-fixed mice. D1- or D2- cre mice were injected with AAV.hSyn.Flex.GCaMP6f.WPRE.SV40, and implanted with an optical fiber terminating in the TuS. Mice also received a headbar for later fixation. Odors were delivered directly to the animal's nose, and respiration was recorded with an extranasal flow sensor. Image made with BioRender. **B.** Optic fiber implant locations in the TuS across D1- and D2-cre mice. **C.** GCaMP activity of D1 and D2 neurons in the TuS during spontaneously-evoked sniffing. **Ci.** Averaged z-scored ΔF/F of D1 and D2 neurons aligned to spontaneous sniff bout onset (D1, $n=4$, 2 points/mouse. D2, $n=5$, 2points/mouse. Overlaid box plots represent average bout duration. **Cii.** Average peak of GCaMP evoked z-scored activity during spontaneous sniffing. **Ciii.** Mean sniffing instantaneous frequency during spontaneous bouts. **Civ.** There was no correlation between GCaMP levels in D1 neurons (peak z-score during a bout) during spontaneous sniffing and (average sniff frequency during the bout, $p>0.05$. **Cv.** There was a significant positive correlation between GCaMP levels in D2 neurons during spontaneous bouts and sniffing frequency ($p<0.0001$). **D.** GCaMP activity of D1 and D2 neurons in the TuS during odor-evoked sniffing. **Di.** Average instantaneous sniffing frequency of both D1-cre ($n=1$, 2 sessions/mouse) and D2-cre ($n=5$, 2 sessions/mouse) mice across repeated odor presentations, with individual mouse data across trials shown in light grey. **Dii.** Averaged z-scored ΔF/F across 4 odor presentations in D1-mice. Odor duration depicted by horizontal line. **Diii.** Averaged peak of the z-scored GCaMP response in D1-cre mice across trials. **Div.** Averaged z-scored ΔF/F across 4 odor presentations in D2-mice. Odor duration depicted by horizontal line. **Dv**. Averaged peak of the z-scored GCaMP response in D2-cre mice across trials. **Dvi.** Overlayed averages of peak z-score GCaMP responses from D1- and D2-cre mice across trials. Data in (Ci),(Dii) and (Div) smoothed for visualization purposes only.

Figure 9. Dopamine binding to D1 and D2 ventral striatum receptors contributes to sniffing. A. Bilateral cannulae implant locations in the TuS and NAcSh. Colored for visualization purposes only. Position relative to bregma. B. Diagram of pharmacological manipulation and behavioral paradigm. Animals were implanted with stainless steel, bilateral cannulae with tips terminating in the TuS ($n=13$) or NAcSh ($n=13$). After surgical recovery, animals underwent behavioral testing. In a counterbalanced, within-subjects design, animals were administered an intracranial infusion of a selective D1, D2, or D3 antagonist or corresponding vehicle control 10min prior to being placed in the plethysmograph. Vehicle = sterile saline + 0-12% DMSO. During a behavioral session, animals were presented with both olfactory and non-olfactory (buzz) stimuli. Image made with BioRender. **C.** Impact of selective antagonism of D1- (Ci), D2- (Cii), and D3-receptors (Ciii) on spontaneous sniffing. D3 antagonism had no effect on spontaneous sniffing in the TuS or NAcSh (Ciii, $p>0.05$). **D.** Impact of selective antagonism of D1- (Di), D2- (Dii), and D3-receptors (Diii) on odor-evoked sniffing. D1 and D3 antagonism had no effect on odor-evoked sniffing in the TuS or NAc (Di & Diii, $p>0.05$). **E.** Impact of selective antagonism of D1- (Ei), D2- (Eii), and D3-receptors (Eiii) on buzz-evoked sniffing. D2 and D3 antagonism had no effect on buzz-evoked sniffing in the TuS or NAc (Eii & Eiii, $p>0.05$). Data are mean (dark bolded line) ± SEM, lighter

1648 lines = individual mice. Abbreviations: SCH (D1 antagonist SCH23390), RAC (D2 antagonist
1649 raclopride), PG0 (D3 antagonist PG010370), VEH (vehicle). ****p<0.0001, **p<0.01, *p<0.05.
1650

Johnson et al., Figure 1

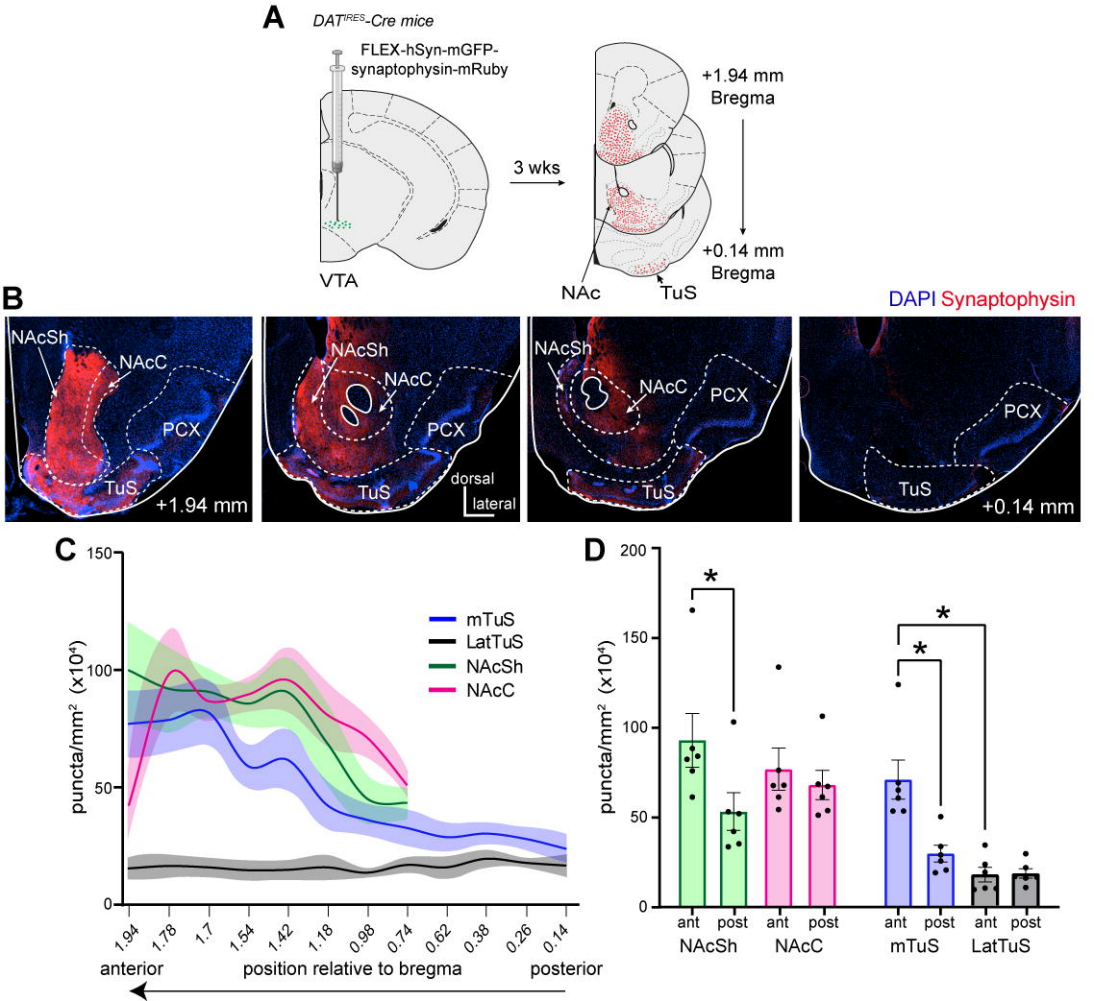

Johnson et al., Figure 2

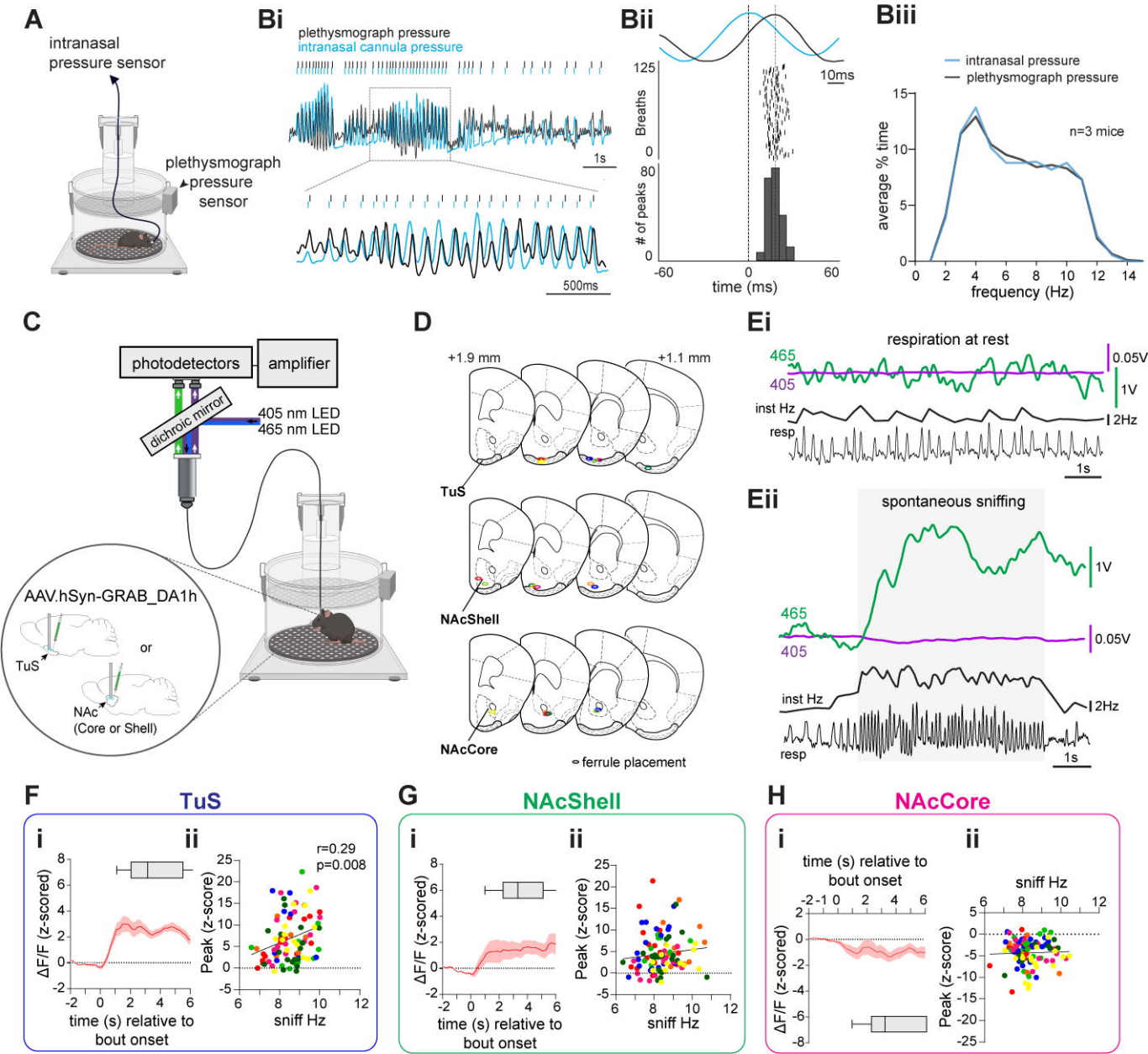

Johnson et al., Figure 3

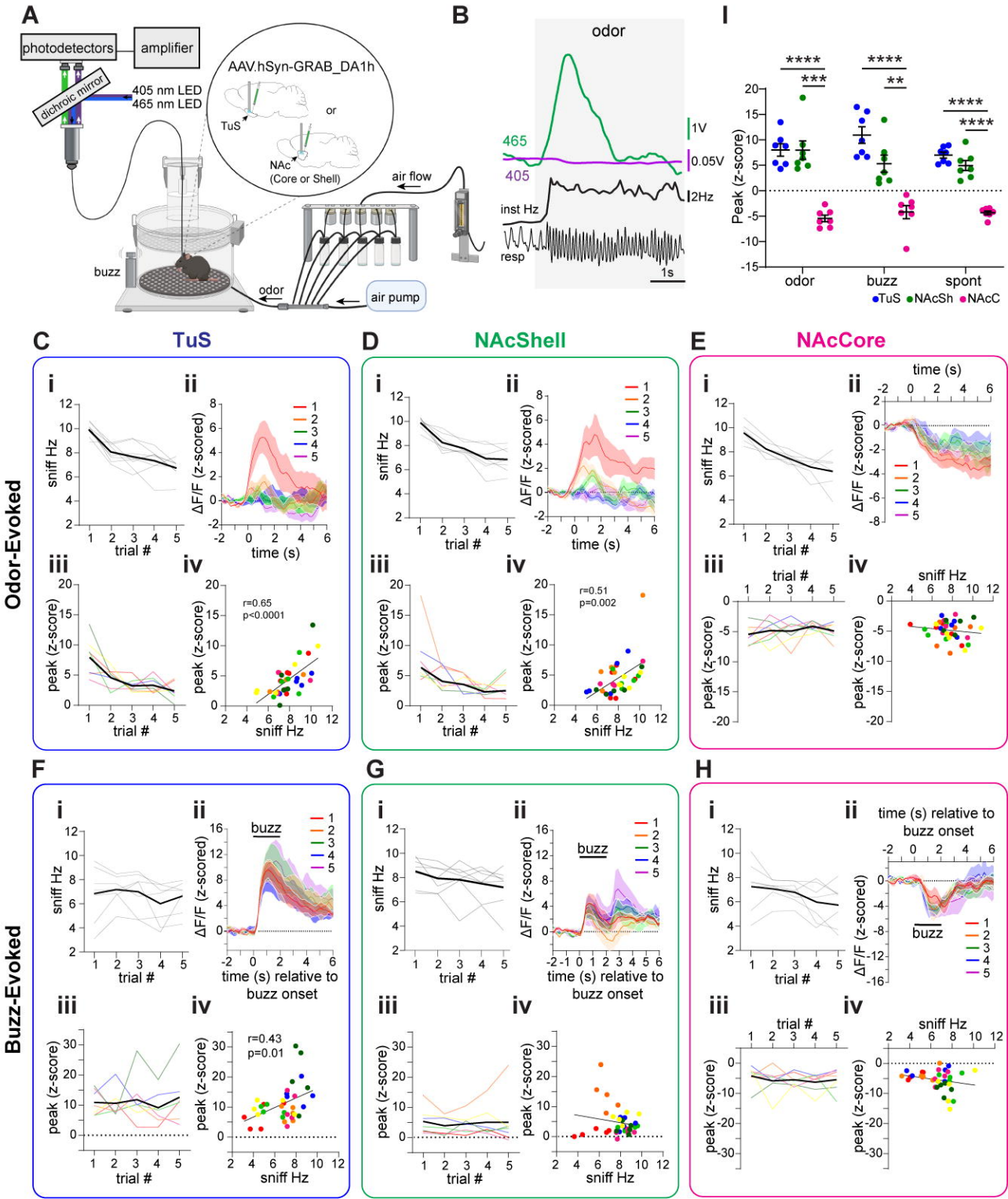

Johnson et al., Figure 4

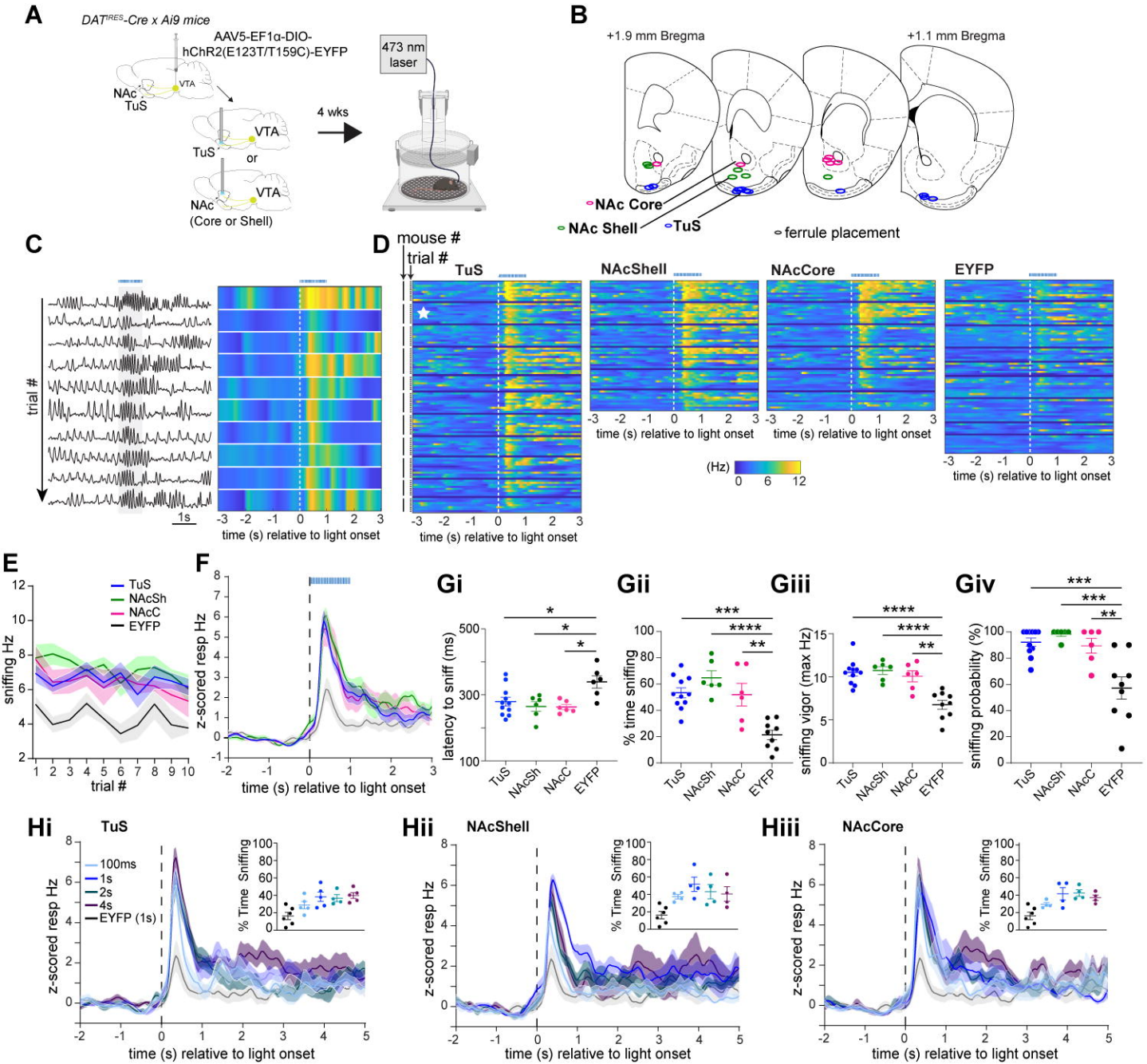

Johnson et al., Figure 5

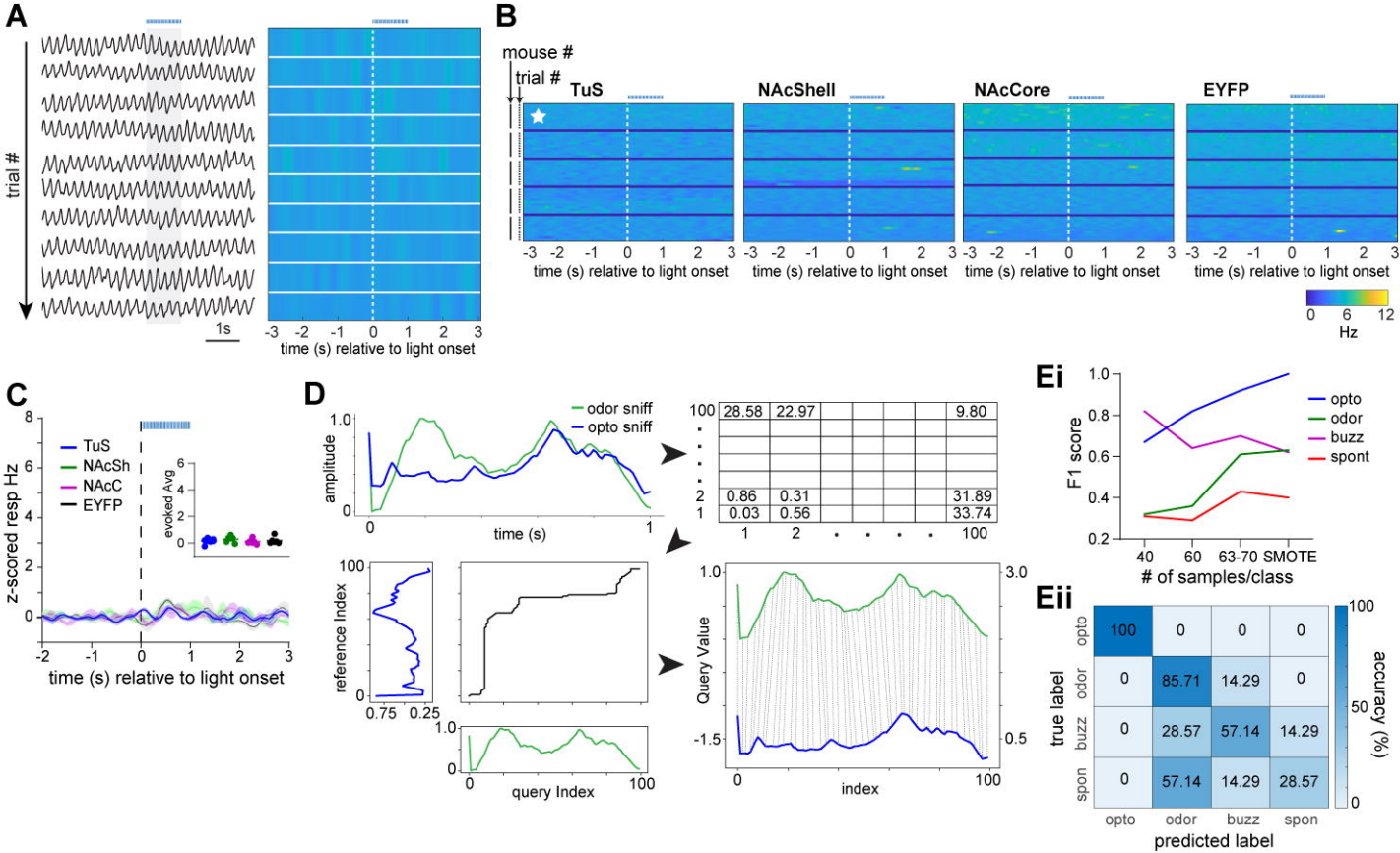

Johnson et al., Figure 6

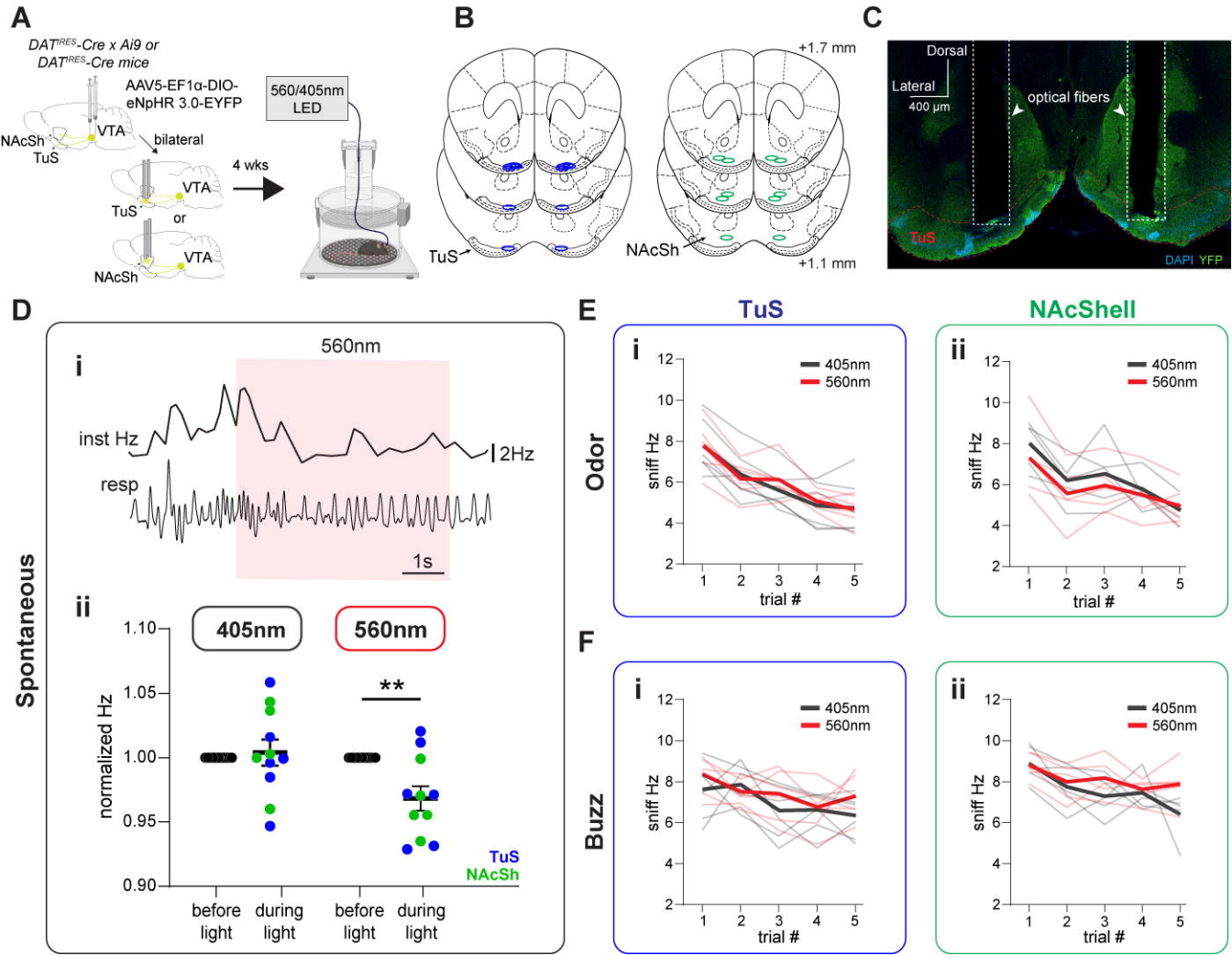

Johnson et al., Figure 7

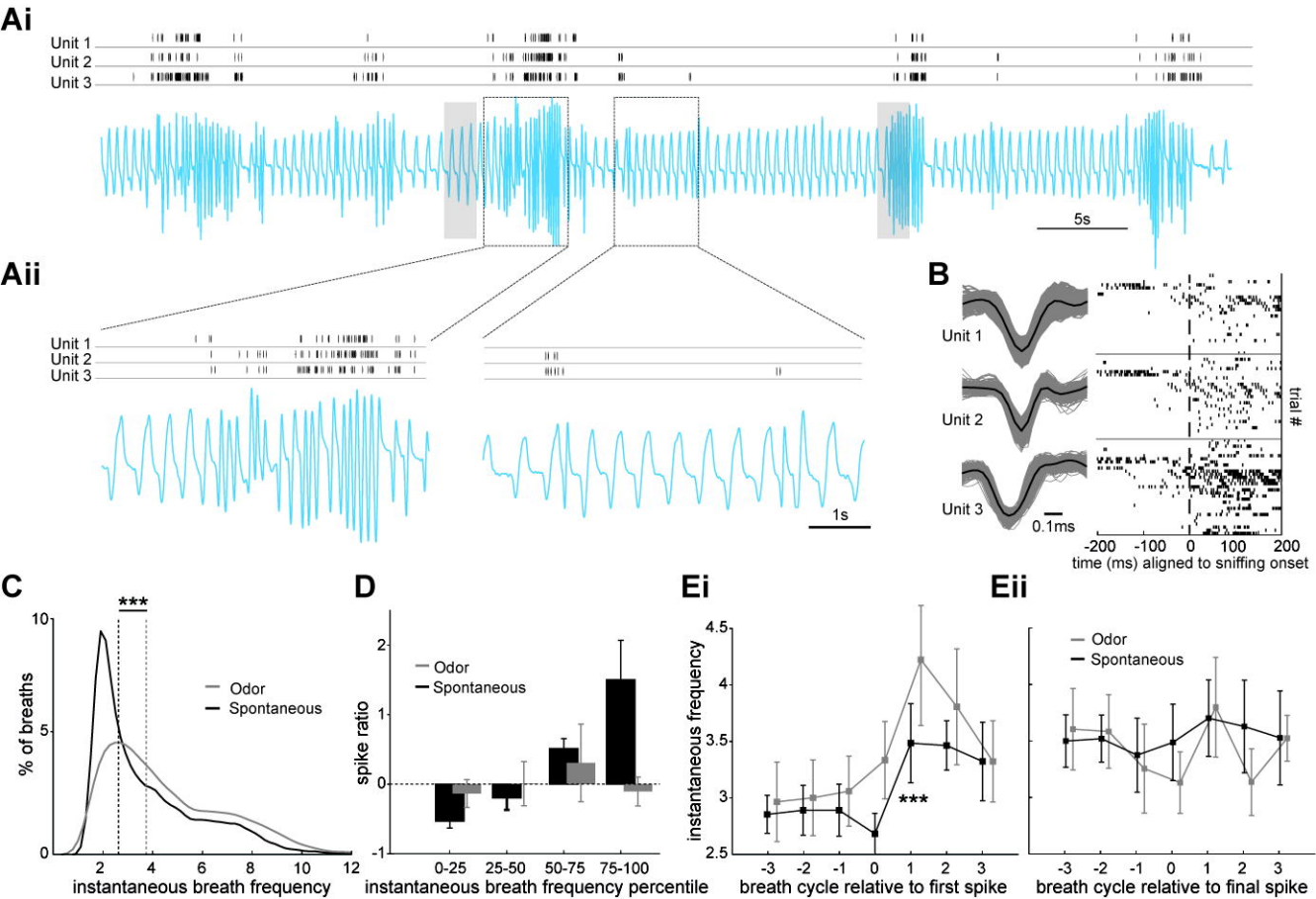

Johnson et al., Figure 8

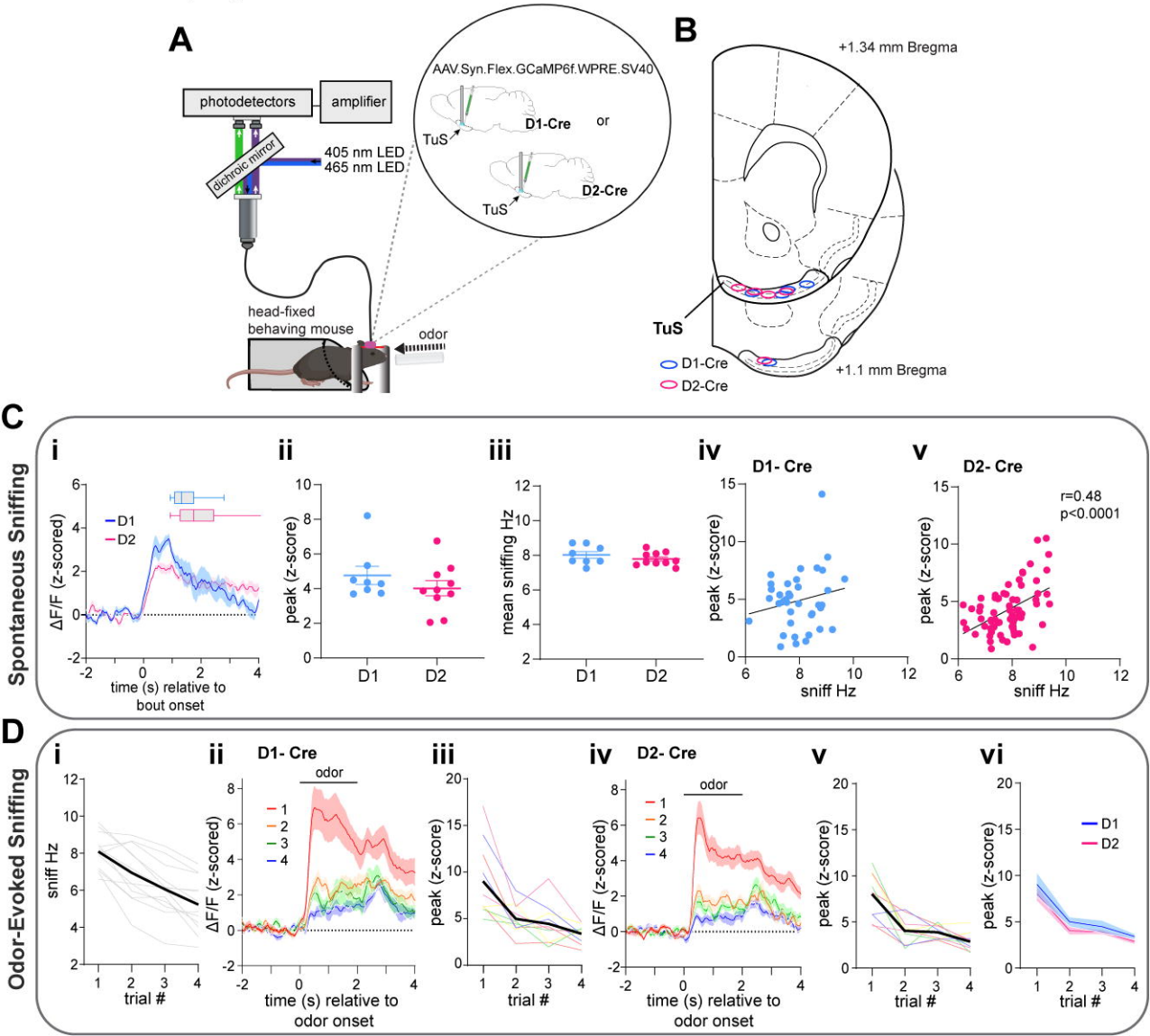

Johnson et al., Figure 9

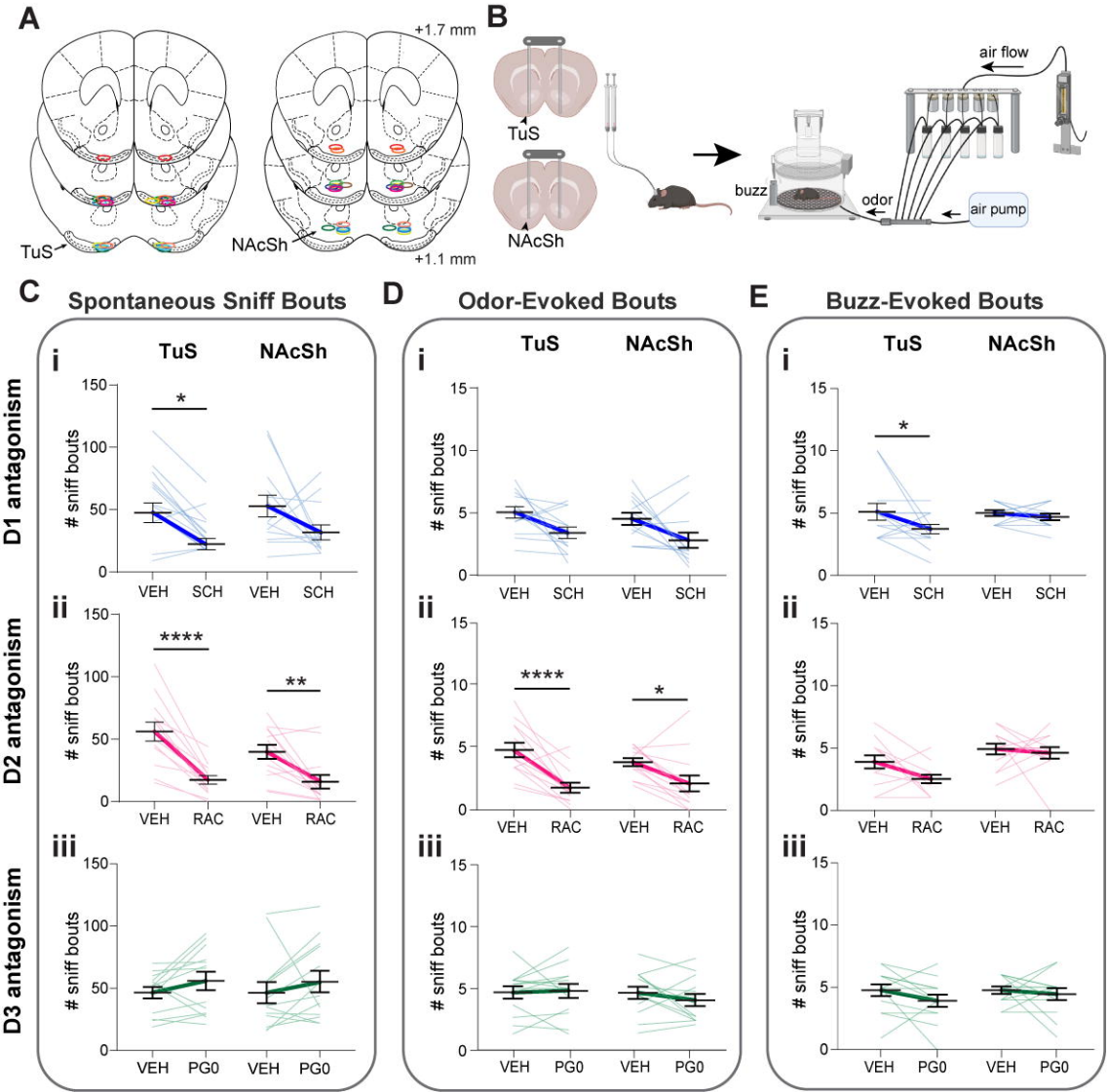

Johnson et al, Supp Figure 1

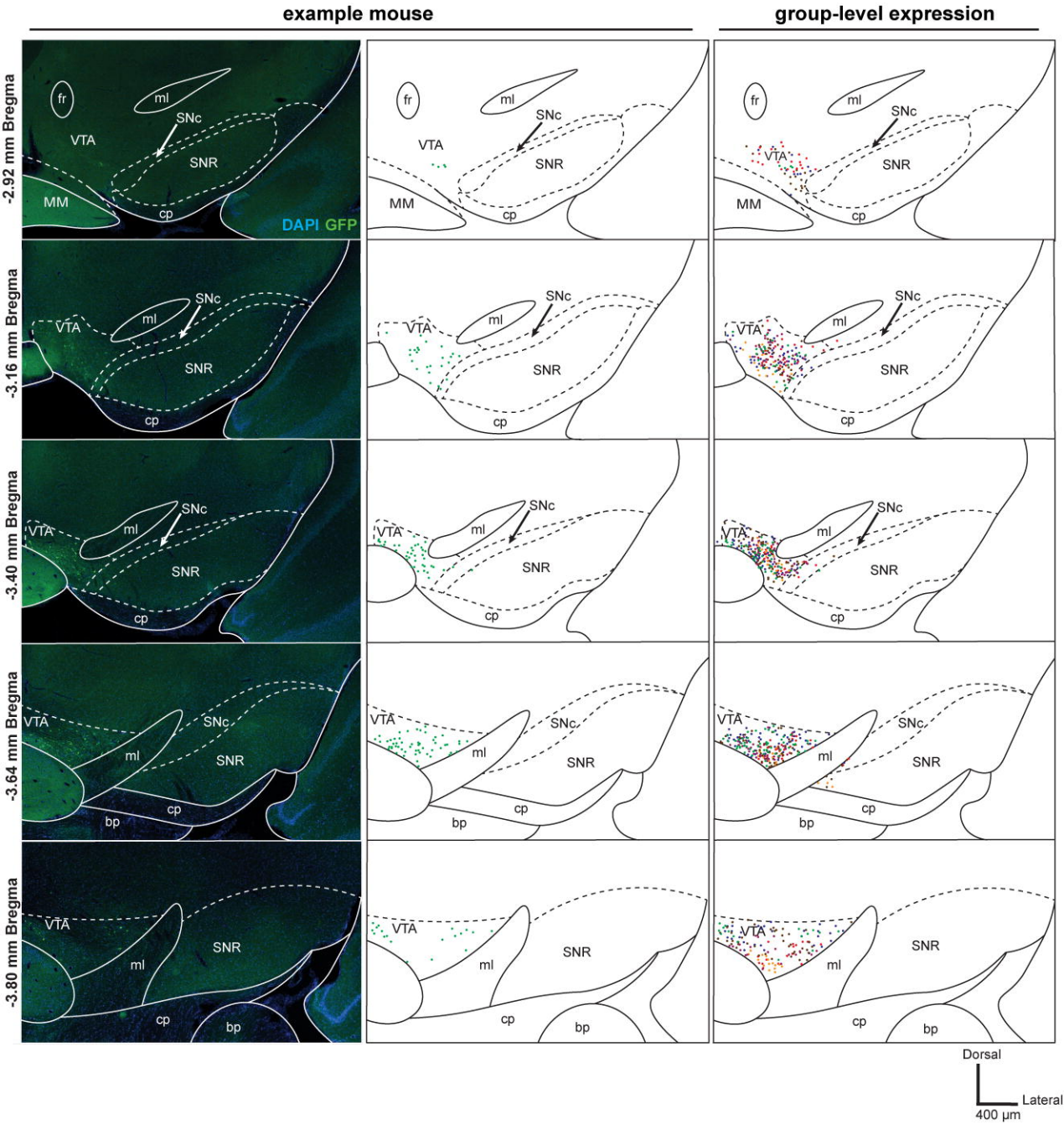

Johnson et al, Supp Figure 2

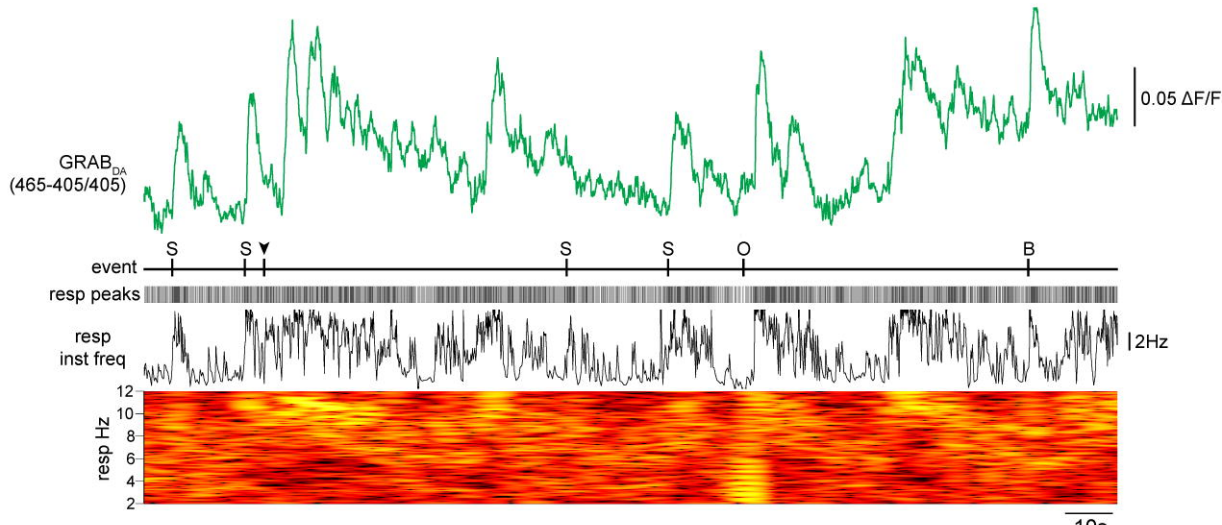

Johnson et al., Supp Figure 3

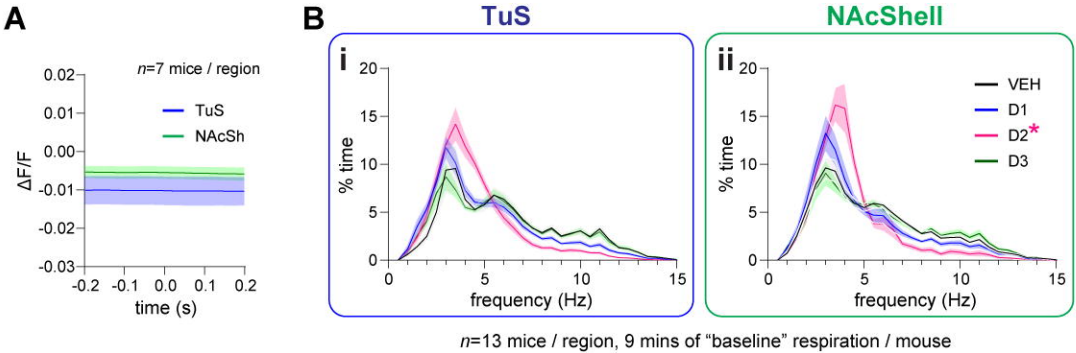

Johnson et al., Supp Figure 4

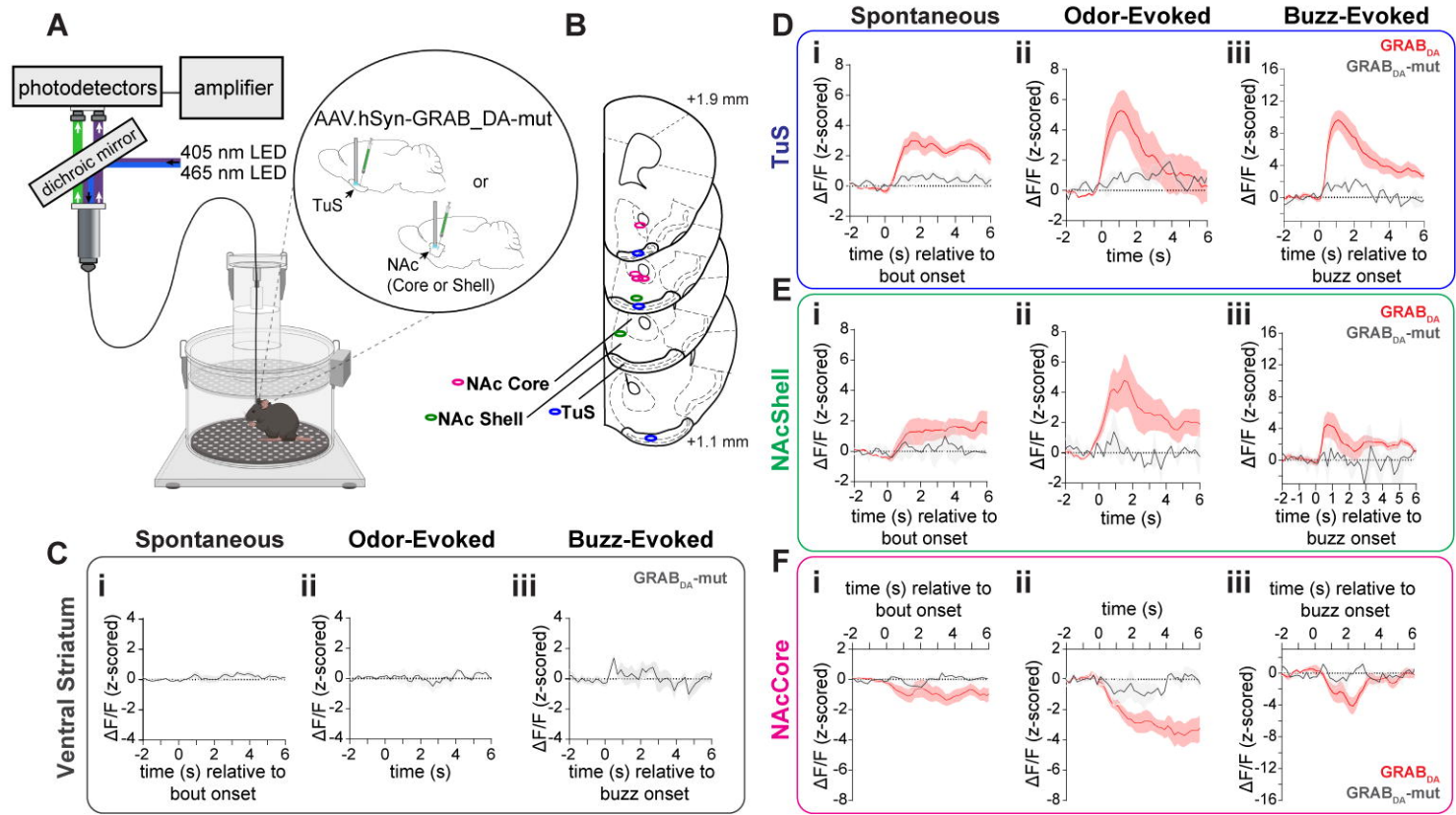

Johnson et al, Supp Figure 5

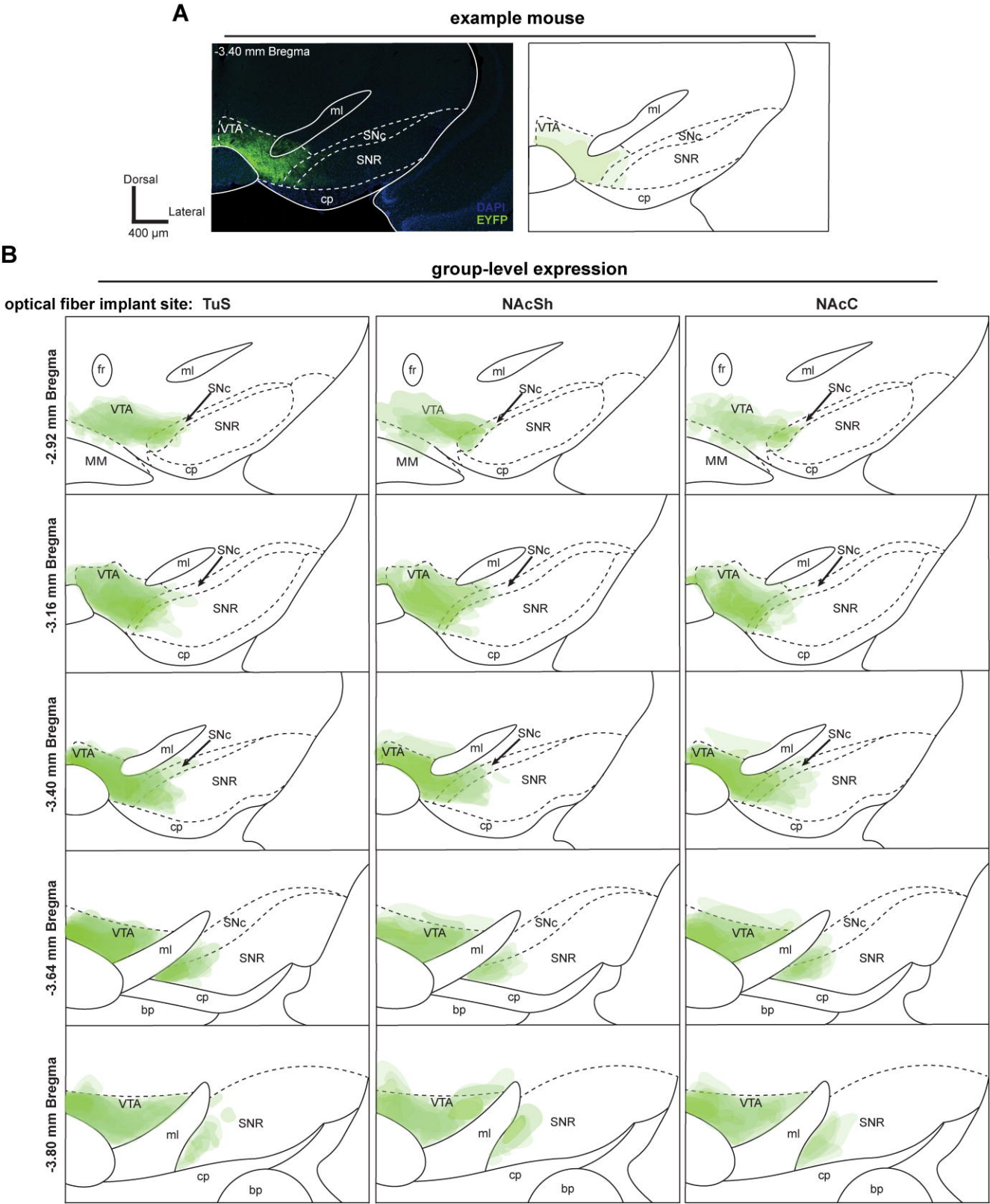

Johnson et al., Supp Figure 6

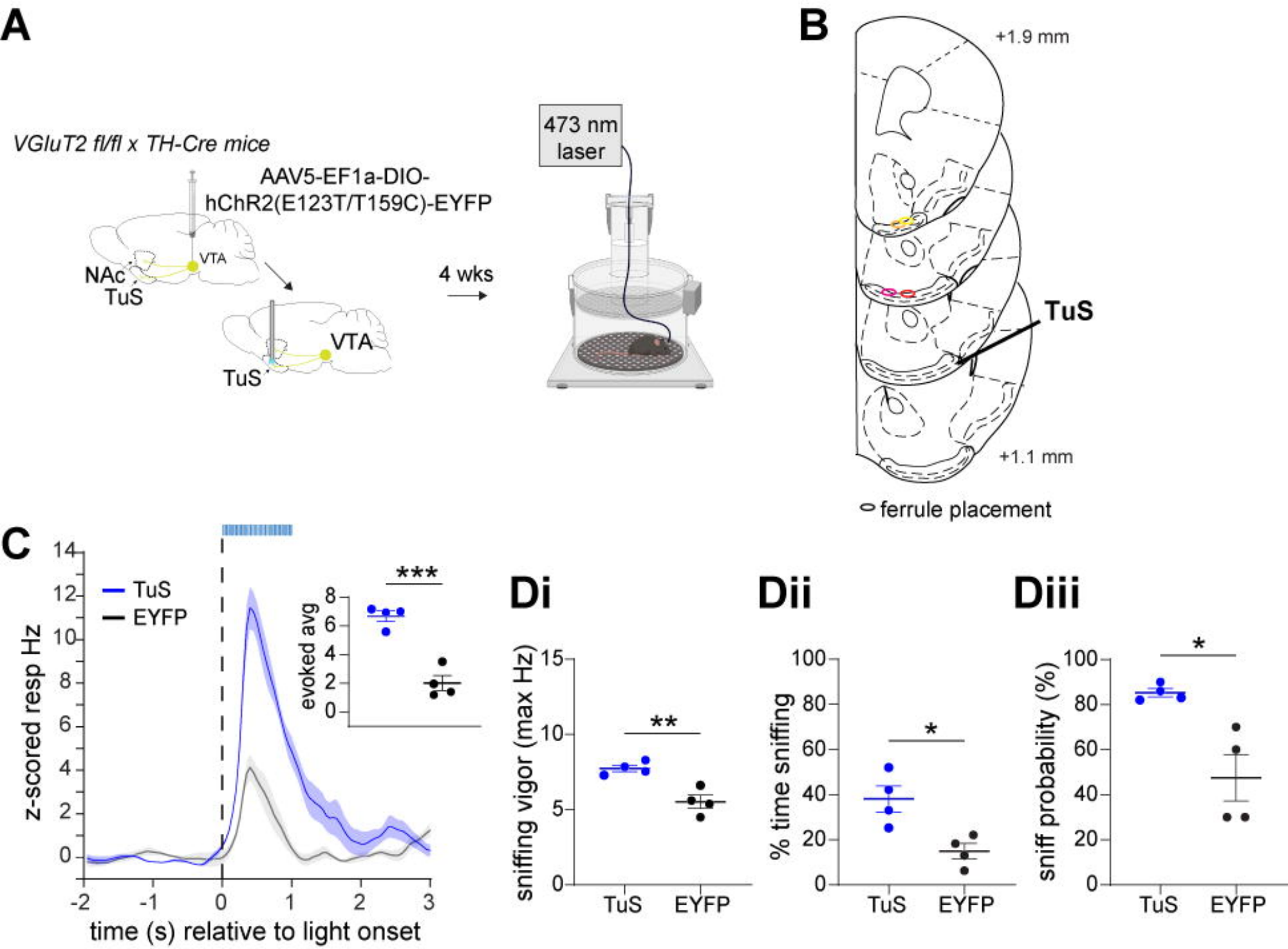

Johnson et al., Supp Figure 7

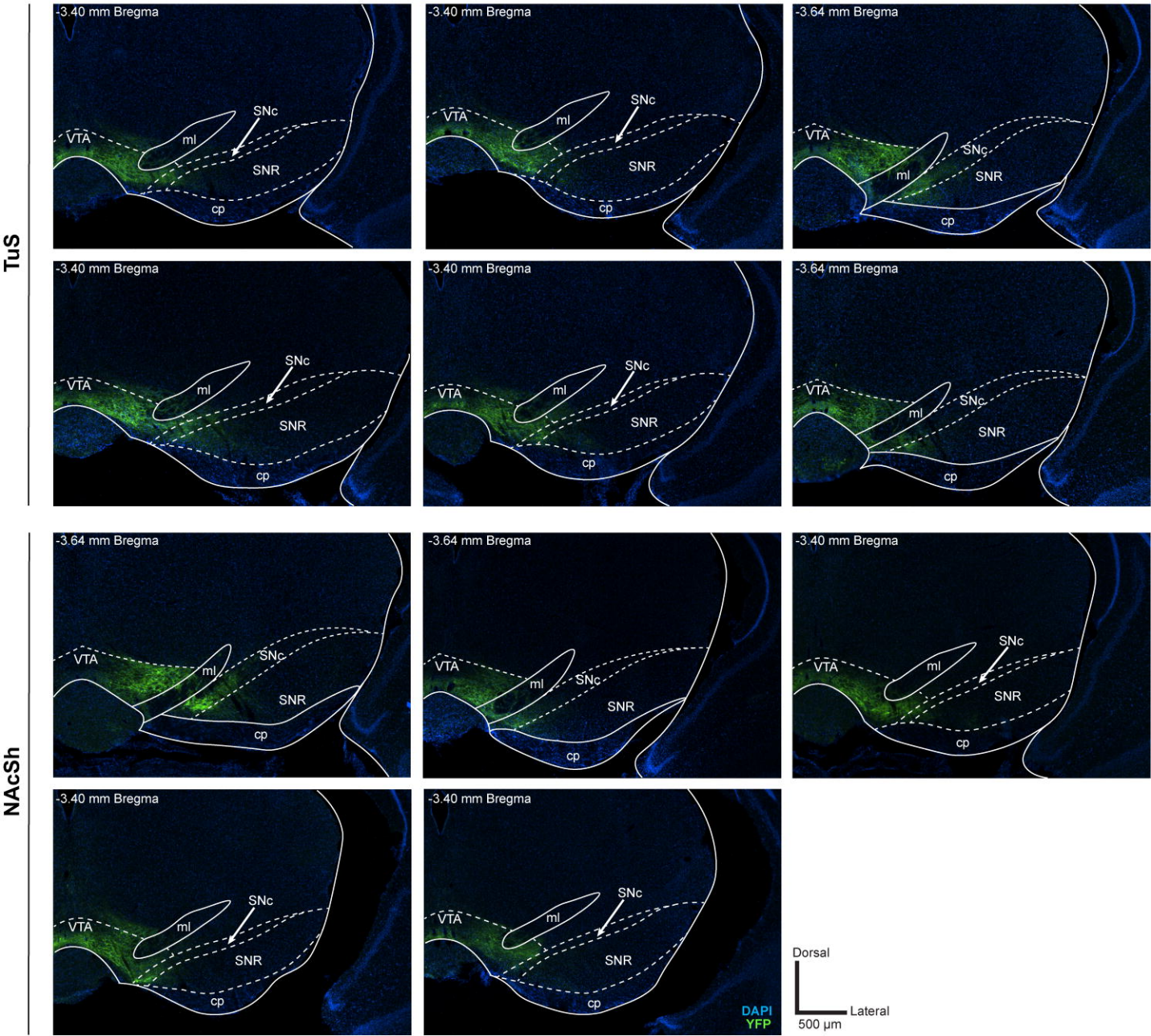
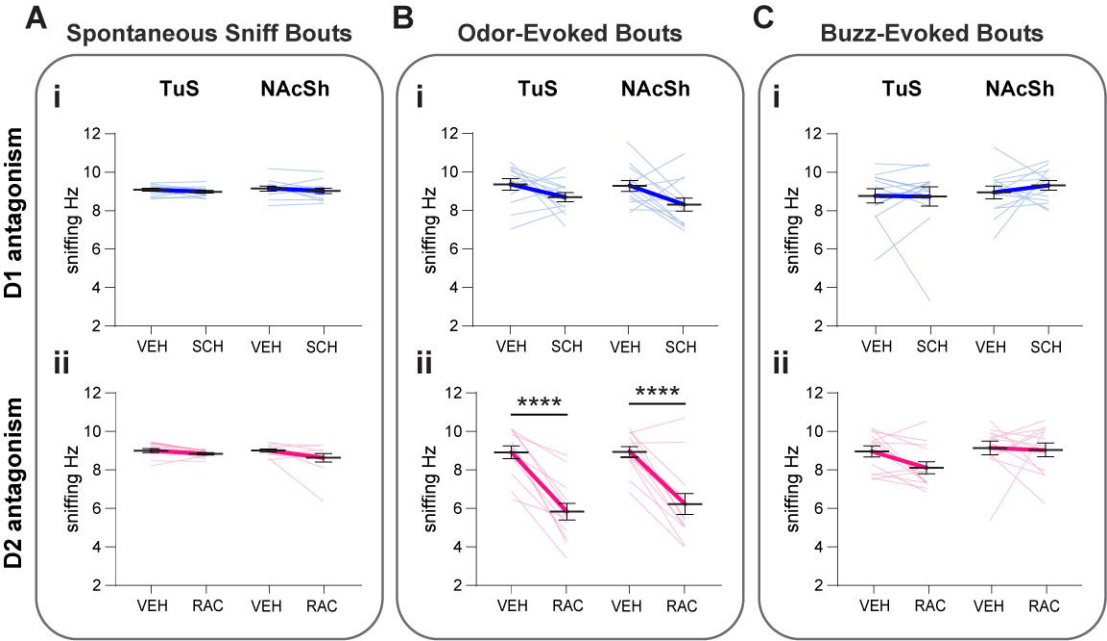
Johnson et al., Supp Figure 8